To the Graduate Council,

I am submitting herewith a thesis written by Anshul Kumar Singh entitled “Laser In-Situ Combinatorial Carbide Coating on Steel.” I have examined the final electronic copy of this thesis for form and content and recommend that it be accepted in partial fulfillment of the requirements for the degree of Master of Science, with a major in Materials Science and Engineering.

Narendra B. Dahotre
Major Professor

We have read this thesis and
recommend its acceptance:

Craig A. Blue

Peter K. Liaw

Accepted for the Council:

Anne Mayhew

Vice Chancellor and
Dean of Graduate Studies

(Original signatures are on file with official student records.)

LASER IN-SITU COMBINATORIAL CARBIDE COATING ON STEEL

A Thesis
Presented for the
Master of Science
Degree
The University of Tennessee, Knoxville

Anshul Kumar Singh
August 2004

Dedicated

To

My parents and sister

ACKNOWLEDGEMENTS

I would like to express deepest gratitude to my major advisor Dr. Narendra B. Dahotre for his guidance, never ending support and motivation throughout this study. I would always be indebted to him for inculcating the spirit of "Keep going on..." in me.

I would like to take this opportunity to sincerely thank Dr. Craig Blue and Dr. Peter K. Liaw for serving on my thesis committee. I also give a special thanks to Wallace D. Porter for access to his laboratory and for his help and guidance with the DSC experiments. I express my sincere thanks to Dr. Joseph Spruiell for permission to use and assistance with the XRD facility in his lab. I am thankful to Dr. Gajanan Bhat for access to his laboratory for the TGA experiments.

I would also like to acknowledge the thermal analysis (DSC) sponsored by the Assistant Secretary for Energy Efficiency and Renewable Energy, Office of FreedomCAR and vehicle technologies, as part of the High Temperature Materials Laboratory User Program, Oak Ridge National Laboratory, managed by UT-Battelle, LLC, for the U.S. Department of Energy under contract number DE-AC-05-00OR22725.

I want to acknowledge all my colleagues S Nayak, Abhijeet Khangar, Greg Engleman, Anil Kurella and Raghuvir Singh for their suggestions and continuous help during the study.

Lastly, I would like to thank my family and friends, whose continuous encouragement made this work possible.

ABSTRACT

The potential for synthesizing an *in-situ* grown ultra-fine carbide composite coating on the surface of steel during laser surface engineering was investigated. A 2.5 KW Nd:YAG laser was employed to modify the surface of a AISI 1010 steel deposited with a precursor powder mixture of Fe, Ti, Cr and C. With the help of laser surface engineering, carbide composite coating on the surface of plain C steel was achieved. It is envisioned that such a coating will offer superior tribological properties.

Energy Dispersive Spectroscopy in supplement with X-ray Diffractometery indicated the evolution of TiC, Fe-Cr, and M_7C_3 as major phases in the coating. An oscillatory pattern for evolution of M_7C_3 was observed with respect to the laser power over the range of 900-2100 watts during processing. Although TiC was present in all the samples, the chromium carbides were absent in samples processed at certain laser powers. Corresponding to this behavior, variation in mechanical properties of the coating was observed. The hardness and wear properties of the samples without chromium carbides was inferior in comparison to samples with both TiC and chromium carbides.

The roles of *in-situ* growth, refractory nature of the carbide particles, the non-equilibrium nature of the process and their contribution in successfully forming a composite coating have been described. Computational techniques were employed with the aim of studying possible reasons for phase evolution, stability of phases and solidification path and thus optimize parameters to tailor properties according to requirement. The temperature range of thermal transitions within the quaternary system

(Fe, Ti, Cr and C) and the thermal stability of the evolved phases were studied with the help of differential scanning calorimetry (DSC). DSC studies indicated that the major exothermic reactions (formation of carbides) take place within 850-1150^{o}C. Temperature ranges for individual reactions were investigated. The evolved phases (TiC, M_7C_3, Fe-Cr and Fe_3C) were characterized using X-ray diffraction (XRD). This multicomponent powder mixture, which was used as a precursor for synthesizing a composite coating on the surface of steel via laser surface engineering (LSE), was computationally investigated for thermal stability. The intended wear applications of the coating made thermal stability investigations imperative, as there is a localized heat buildup during wear, because of the contact between rubbing surfaces. Experimental evaluation (DSC) of thermal stability of the phases formed was done to supplement the computational investigations. The degradation of the coating due to prolonged stay at elevated temperatures (in oxidizing environments such as air) could lead to degradation in the properties of the coating. High temperature oxidation studies were done to investigate the oxidation kinetics of the composite coating.

Table of Contents

1. INTRODUCTION **1**

2. LITERATURE REVIEW **4**

2.1 Background 4

2.2 Surface Engineering 6

2.2.1 Laser Surface Engineering *7*

2.3 Materials System 9

2.3.1 Substrate *9*

2.3.2 Coating Elements *10*

2.4 Phase Evolution: Computational Approach 14

2.5 Differential Scanning Calorimetry 16

2.6 High Temperature Oxidation 18

2.7 Flow Diagram 20

3. EXPERIMENTAL PROCEDURE **22**

3.1 Laser Processing 22

3.2 Characterization 25

3.2.1 Microstructural Characterization *25*

3.2.2 Structural Characterization *25*

3.3 Computational Thermodynamic Calculations 26

3.4 Differential Scanning Calorimetry 27

3.5 Functional Properties 30

3.5.1 Microhardness Results *30*

3.5.2 Wear Studies *31*

3.5.3 High Temperature Oxidation Analysis *31*

4. RESULTS AND DISCUSSION **33**

4.1 Microstructural Evolution 33

4.2 Phase-Structure Dependence on Laser Processing Power..... 41

4.3 Prediction and Verification of Phase-Structure Evolution 49

4.3.1 Computational Thermodynamic Evaluations *49*

4.3.2 Analytical Evaluation: Differential Scanning Calorimetry *60*

4.4 Processing Effects on Functional Properties. 75

4.4.1 Hardness *75*

4.4.2 Wear Performance *76*

4.4.3 Oxidation Kinetics *78*

5. SUMMARY **85**

6. SUGGESTIONS FOR FUTURE WORK **89**

REFERENCES **91**

VITA **98**

List of Tables

Table 1: Composition of AISI 1010 steel (all elements in wt%). 9

Table 2: Mechanical properties of AISI 1010 steel at 25^{o}C 10

Table 3: Processing parameters used for laser treatment. 24

Table 4: Sample specifications and conditions used during DSC. 27

Table 5: List of various phases identified during XRD. 44

Table 6: Free energy of reaction as function of temperature. 45

Table 7: Ratio representing an approximate estimate of the relative amount of Fe-Cr present in samples processed at various powers. 47

Table 8: Variation of amount of phase with (a) Fe/Cr and (b) Fe/Ti ratios. 57

Table 9: Evaluation of separated peaks obtained by de-smearing of twin exothermic DSC events. 72

Table 10: Oxidation kinetic constants for composite coatings at 700 ^{o}C. 83

Table 11: Oxidation kinetic constants for composite coatings at 1000 ^{o}C. 84

List of Figures

Figure 1: Flow diagram of the investigation..... 21

Figure 2: Process schematic depicting the steps involved in the process. 23

Figure 3: Schematic of the heating process in the Infrared furnace. 29

Figure 4: Scanning electron micrograph of sample processed at 1500 W (a) higher magnification overview of the cross-section and image of (b) substrate, (c) transition zone and (d) coating region..... 34

Figure 5: Scanning electron micrographs of the coating (surface composite layer) indicating uniform distribution of in-situ grown particles. 36

Figure 6: SEM image of the coating (1500 W) (a) Higher magnification view and, EDS of (b) the matrix and (c) black particle. 37

Figure 7: X ray Diffraction spectra for samples processed at different laser powers. 42

Figure 8: Variation of free energy of carbides with temperature..... 45

Figure 9: Schematic of reaction products as a function of laser processing power. 48

Figure 10: Calculated phase diagram for the quaternary alloy coating. 52

Figure 11: Solidification path traced using calculations based on Scheil assumptions. ... 53

Figure 12:(a) The multicomponent (Fe-Ti-Cr-C) system phase diagram. (b) Mole fraction of all phases calculated at 1400 K for the current alloy composition. 55

Figure 13: Mole fraction of phases with increasing amount of C in the precursor powder mixture. 58

Figure 14: Calculation of thermal stability of the phases. 59

Figure 15: DSC curves for heating and cooling of the precursor powder mixture at the rate of 40^{o}C/min in Argon atmosphere. 62

Figure 16: DSC heating and cooling curves for re- run of Fe, Ti, Cr and C powder mixture. 64

Figure 17: DSC heating and cooling curves for Ti, Cr and C powder mixture at 40^{o}C/min in Argon atmosphere. 65

Figure 18: XRD spectra for furnace heated samples. (a) 850 ^{o}C, (b) 1025 ^{o}C, (c) 1075 ^{o}C, (d) 1175 ^{o}C. 67

Figure 19: Fitting with 2 peaks of Fraser-Suzuki (asymmetric gauss) profile for DSC twin exothermic event. 72

Figure 20: DSC runs for laser processed coating (processed at 1.5 kW) at 40^{o}C/min in argon atmosphere. 74

Figure 21: Hardness profiles for laser processed samples. 76

Figure 22: Cumulative weight loss as function of time during dry sliding wear. 77

Figure 23: Weight gain as a function of time at (a) 700 ^{o}C and (b) 1000 ^{o}C. 80

Figure 24: Oxidation kinetics for composite coatings at (a) 700 ^{o}C and (b) 1000 ^{o}C. 82

List of Abbreviations

LSE	Laser Surface Engineering
SEM	Scanning Electron Microscopy
EDS	Energy Dispersive Spectroscopy
XRD	X-ray Diffractometery
DSC	Differential Scanning Calorimetry
HAZ	Heat Affected Zone
TGA	Thermogravimetric Analysis
TiC	Titanium Carbide
FCC	Face Centered Cube
BCC	Body Centered Cube
M_7C_3	M= $(Cr, Fe)_7C_3$

List of Symbols

T	Temperature
ΔT	Undercooling
I	Rate of Nucleation
α	Ferrite
α'	Martensite
γ	Austenite
ΔG	Free Energy Change
a	Lattice Parameter

Chapter 1

1. INTRODUCTION

The importance of surface properties is foreseeable with the decreasing size of most modern equipments. The achievement of better surface properties (tribological, oxidation, etc.) remains to be a great challenge. As development of novel materials with superior properties goes on, modification and tailoring of the surface of currently available materials might be the most effective approach. The modification of surface layers is advantageous both in terms of cost and the application desired. Conventionally, it is a known fact that grain refinement leads to substantial improvement in strength, hardness, ductility and toughness of a bulk material. Grain boundary hardening is one of the most desirable ways for property improvement. The same argument can be extended to ultra hard surface coatings as well. As the grains size decreases i.e. dislocation movement is hindered and hardening of material takes place by the conventional 'Hall Petch' relation. Also, grain sliding and geometric adjustments improve ductility. But this scenario holds good only till the grain size is bigger than a few 10's of nanometers (~100nm) as at sizes smaller than that, grain boundary sliding starts to dominate and hence a drop in the strength is observed [1]. The decrease in strength or softening can be attributed to the concentration of lattice defects in grain boundaries, which under stress allows faster diffusion of atoms and vacancies. Hence, if grain boundary diffusion dominates over bulk diffusion, softening can be expected. Another important property while forming a hard coating for tribological applications is toughness. Grain boundary diffusion and sliding

might have a positive effect on it. Therefore, it is necessary to design a coating in which both hardness and toughness are optimized. One way to achieve this is to introduce a hard phase within a tough metal matrix. The hard phase could be very fine carbide particles.

The present work attempts to simultaneously synthesize a combination of carbide coatings (Ti and Cr based). The aim is to employ the Fe-Ti-Cr-C quaternary system to engineer the surface of plain carbon steel for *in-situ* formation of both Ti and Cr based carbides using Laser Surface Engineering (LSE). The extremely high flux of energy, applied by a laser to a very thin surface layer of a specimen, produces a highly localized heat source capable of engineering the microstructure and hence properties of various materials. Ultra hard composite coatings produced by this technique are envisioned to be used in heavy-duty off the road transportation vehicles for applications such as earth moving, mining, crushing etc. Currently, such wear resistant surfaces are produced by various surface engineering techniques, among which overlay welding and thermal spray methods are frequently used. Although there is no problem of debonding with overlay welding, it has a inherent drawback of excessive heating of the substrate which effects its properties. On the other hand, during thermal spray, there is no difficulty of disproportionate heating of substrate, but it has a critical problem of debonding of particles from the matrix. In comparison, during in-situ synthesis of carbides using laser, these difficulties do not exist and a metallurgically sound, uniform coating is achieved which has superior surface properties.

The coating has been characterized for microstructural, structural, mechanical and tribological properties. Computational and analytical invesitgations of the multi-component coating system was done to analyze the phase evolution pattern, reaction path,

thermal stability of the phases to eventually develop a thorough understanding of the quaternary system involved. Thermogravimetric analysis was performed to investigate the oxidation kinetics of the coating. The dissertation is divided into 6 chapters. The first chapter gives a brief introduction of the research topic, the second chapter presents the background of the process and the hypothesis behind the processing and characterization of the coating, the third chapter gives the experimental details for laser processing and characterization techniques, the fourth chapter presents and discusses the results and thereafter the fifth chapter summarizes the whole study. The sixth chapter presents some suggestions for future work, to further comprehend the coating system.

Chapter 2

2. LITERATURE REVIEW

2.1 Background

Wear is a major problem in various industrial applications and the development of novel wear resistant materials is therefore both technically and economically advantageous. Introduction of hard particles in a metal can considerably decrease the amount of abrasive wear [2]. Large amount of carbides are contained in high Cr white cast irons [3,4] and high speed steels and these materials are widely used in number of industries where resistance to wear is required. The carbides, like M_7C_3 (M=Fe,Cr) in high Cr white irons are hard (1500-1800 HV), which makes them an attractive class of material for wear applications. The superior wear resistance is accompanied by poor impact resistance which might restrict their use in many applications. But, it can be interpreted that the introduction of hard particles in a tough, chemically compatible matrix can aid in the development of such materials.

Metal matrix composites bring new possibilities of wear resistant materials. Generally, metal matrix composites reinforced with ceramics have excellent properties compared to un-reinforced metals because they exhibit high strength, elastic modulus and improved wear resistance. Composites with steel matrix and metallic carbides offer high hardness and sufficient fracture toughness. The carbide particles have exceptionally high hardness and are frequently incorporated as reinforcements. By careful selection of the type of carbide, it is possible to design a composite for severe abrasive conditions.

Among the most commonly used carbides are titanium, tungsten and chromium carbides. The respective Vickers hardness of these carbides is 2900-3200 kg/mm^2 [5], 1730 kg/mm^2 [6] and 1500-1800 HV [2] respectively. This indicates that the carbides are extraordinarily hard and can act as good reinforcement for wear resistant applications. But, for wear resistance to be maintained at elevated temperatures, the carbides need to be thermally stable. Titanium carbide is refractory in nature and decomposes at very high temperatures (3065^{o}C) [7]. Tungsten carbide readily decarburizes at temperatures greater than 500 ^{o}C [8] while chromium carbide remains stable to beyond 1000 ^{o}C. TiC is a proven reinforcement in iron or nickel based alloys due to its high hardness and thermodynamic stability [9,10]. Another key aspect to be considered is the fine size, uniform distribution of the carbide particles and good interfacial bonding with the matrix to avoid spalling of the particles. Hence the route technique chosen for incorporating the particles also plays a very important role.

Typically, TiC reinforced composites are fabricated by powder metallurgy route using TiC powders along with steel powders [11,12,13] .To achieve homogeneous mixing, casting of liquid Fe-Ti-C alloys [14,15] , Fe-Ti and Fe-C alloys [16,17] or Fe-Ti alloys and graphite [18] to form *in-situ* carbides has been reported in the past. Other fabricating techniques include liquid phase sintering [19] and self sustaining high temperature synthesis [20]. The *in-situ* growth of carbide particles has 3 major advantages. The problem of contamination can be avoided as the particles are grown from within the liquid and not handled at any stage of processing. The cost of the operation is reduced as the number of steps involved during the process is minimized. Most importantly, better interfacial bonding between particles and matrix can be achieved due to the *in-situ*

growth of the carbide. Such composite can be synthesized as bulk material or surface coating. Synthesis of surface composite coating holds tremendous promise in terms of savings in material and cost.

2.2 Surface Engineering

The resulting composite is being formulated for wear resistant applications. The surface properties are more important rather than bulk properties for such applications. The targeted application can be achieved by forming a surface composite coating rather than a monolithic composite which is expensive. This in turn has another advantage that the surface of a commonly available inexpensive material can be modified to achieve the desired properties. The fabrication and development of expensive alloys for specific applications can thus be avoided. Among the commonly used surface engineering techniques is thermal spray coating [21,22], chemical and physical vapor deposition (CVD and PVD) [23,24], ion implantation [25,26], direct irradiation with a high energy electron beam [27,28]. Recently attempts have been made to form laser surface engineered coatings for such applications. [29,30]. The technique of surface modification depends upon the substrate materials, and the particular application requirements, particularly the design stress level and flaw tolerance. At moderate loads, protection can be provided by means of CVD and PVD processes, wherein the layer thickness amounts to several microns [31]. However, at high contact loads, a thicker and well-bonded hardened layer is required, which can be provided by means of plasma spraying and laser processing. These techniques are capable of modifying the surface layer over several hundred microns [32,33].

2.2.1 Laser Surface Engineering

LSE is a technique for improving surface related properties (viz. hardness, wear, oxidation/corrosion resistance) by modification of the surface layer of a bulk component using laser as the source of energy. The melt pool generated due to interaction of laser beam with the material undergoes rapid solidification, which provides a unique opportunity for non-equilibrium synthesis of materials. The volume of melt pool coupled with conduction mode of heat transfer enables synthesis of highly refined microstructure. Even metastable phases, which are not easily attainable by conventional processes, can be achieved by LSE. Such microstructures are known to have higher hardness, superior wear and oxidation properties. The greatest advantage of this process is that the surface structure can be designed as per the requirements of the application by varying the processing parameters, which include beam power, beam size, scan speed and the composition of the precursor.

The laser beam is a coherent source of light. The emitted light is highly monochromatic which enables efficient focusing. The coherent nature of the laser beam allows it to be focused to a small spot, leading to very high energy density [34]. The high flux of energy in a concentrated beam can be used to heat or melt materials locally. The first attempt at laser surface alloying was reported in 1964 [35]. Availability of various kind of lasers such as CO_2, Nd:YAG and excimer in adequate power level and optical fiber delivery system (in case of Nd:YAG laser) has extended usability of laser in surface engineering and many other manufacturing processes. It has been recognized that by its very nature, laser surface engineering has unique advantages over its conventional

counterparts. The characteristics of laser surface engineering which make it a attractive process are rapid processing nature of the process, high energy density due to focused laser light, choice of employing with/without atmosphere control, possible surface treatment of materials difficult to melt (such as ceramics, refractory metals), treatment of precise surface area by simply varying the optics and beam parameters, involvement of little or no contamination, possibility of treating different shapes and non flat surfaces, formation of a metallurgically bonded coating problems avoiding the problems of pores and cracks with conventional coating and lastly the use of fiber-optics makes laser treatment amenable to automation.[36]

The main lasers available in the market for high power applications are continuous wave CO_2 laser (wavelength 10.6μm), Nd:YAG laser (active entity Nd^{+3} with wavelength 1.06 μm) and excimer (wavelength in ArF: 193 nm, KrF: 248 nm, XeCl: 308 nm and XeF: 351 nm). Nd:YAG laser have gained popularity primarily for the flexibility provided by fiber optical beam delivery making it suitable for many applications. High power lasers can be focused onto a very small spot of 0.1 - 1.0 mm. The intensity of the order of 10^{10} W/m^2 can thus be obtained. CO_2 and Nd:YAG laser have successfully been applied for materials processing such as welding, cutting, re-melting and surface alloying.

The localized melting of the surface material during laser treatment makes it possible to treat small surface areas without altering or affecting bulk properties and obviates the need for expensive alloying of the entire component. The high temperature gradients and heat sink effect (of the rest of the components) result in a very high cooling rate or rapid self quench, exceeding 10^{6-8} K/s. [36] Another key feature of laser is that it is a highly controllable source of energy, which can be precisely manipulated by using a

computer. The amount of energy applied, the location, working and nozzle distance, and the scan speed can all be monitored through computer numerically controlled (CNC) machines. [37] Thus processing of a large number of samples of different sizes and materials can be done at a rapid rate.

2.3 Materials System

2.3.1 Substrate

As mentioned earlier, the formation of a surface composite layer makes it possible to use inexpensive and commonly available materials for specialized applications and thus reduce the overall manufacturing cost. The substrate chosen for the current study was AISI 1010 steel. Table 1[38] summarizes the general composition of the plain C steel. Since there are no alloying elements added to the steel, it is an inexpensive and easily available. The mechanical properties of the steel have been tabulated in Table 2. [38] It can be seen that it has good formability and reasonable ductility but it has a very low hardness and hence poor wear resistance.

Table 1: Composition of AISI 1010 steel (all elements in wt%).

C	Mn	P	S
0.08-0.13	0.30-0.60	0.04	0.05

Table 2: Mechanical properties of AISI 1010 steel at 25^{o}C

Property	Value
Density (x1000 kg/m^3)	7.7-8.03
Elastic Modulus (GPa)	190-210
Tensile Strength (MPa)	365
Yield Strength (MPa)	305
Elongation (%)	20
Reduction in Area (%)	40
Hardness (HB)	105

2.3.2 Coating Elements

The aim of the study was to surface engineer the 1010 steel to make it suitable for wear applications. As mentioned earlier, a surface composite layer containing hard carbide particles as reinforcement would be suitable for the job. The quaternary alloy system chosen for surface engineering the substrate was Fe, Ti, Cr and C. Each element had an important role in the coating. The coating elements were chosen with due consideration to inherent advantages of *in-situ* growth of particles. Ti and Cr are known carbide formers. Also, technically there is some solubility of all elements in ferrite, but some elements are not found extensively in the carbide phase. In the absence of carbon, most of the group 2 elements would be found dissolved in ferrite. Therefore, the carbide forming tendency is apparent only when significant amount of C is present in the coating. [39].

With this aim, C was added to the precursor powder mixture. Fe was chosen as the major element in the precursor for the coatings on 1010 steel to avoid any difficulty with chemical compatibility. The carbides have good compatibility and wetting characteristic with Fe [40]. Also, since the substrate is 1010 steel (mainly Fe), good bonding was expected. The effect of Cr, as described by Sidney H. Avner, [39] is that it increases resistance to corrosion and oxidation in steels and in the presence of C, imparts abrasion and wear resistance to the steel. It has been reported in the past that hard facing alloys based on iron are known to have large additions of Cr and C to it. [8]. The microstructure is known to consist of large M_7C_3 carbides in a eutectic mixture of austenite and more M_7C_3. Similarly, as mentioned earlier, high Cr white irons are generally considered to be most abrasion resistant class of materials due to the high volume percent of hard eutectic M_7C_3 carbides. But, these white irons have a problem of poor impact strength which hinders their use. With a steel matrix (which has comparatively higher impact strength) and carbide reinforcements, high wear resistance materials can be developed.

Most of the studies done in the past [11-17] have tried to synthesize only one type of the coating composition, where as on the contrary, the present work attempts to simultaneously synthesize a combination of carbides (Ti and Cr based) in the coating. The present study is aimed at employing the Fe-Ti-Cr-C quaternary system to engineer the surface of plain carbon steel for *in-situ* formation of both Ti and Cr based carbides using LSE (Laser Surface Engineering). During LSE, a part of the substrate along with the pre-deposited precursor layer is melted, mixed and solidified for a modified surface layer. The surface composite thus formed consists of *in-situ* formed carbides, which not

only will improve the hardness and wear resistance of the substrate, but will also have the inherent advantage of being uncontaminated.

With the aim of comprehending the possible phases and develop a background of the materials system, the various related ternary systems were reviewed. This literature review helped in understanding the properties of the stable phases, their stability and hence understanding the phase evolution during the laser assisted surface coating process.

Fe-Ti-C system and TiC:

In this ternary system, Ti depletion occurs with the formation of TiC. As the amount of TiC increases, the activity of Fe increases which leads to the formation of Fe_3C, when Ti concentration falls below a certain critical level. [41]

$$3Fe(l) + TiC(s) \rightarrow Fe_3C(s) + Ti(l)$$

In order to avoid the formation of Fe_3C, the desired level of Ti needs to be maintained. This meant that, while deciding the composition of the precursor, high levels of Ti were desired.

TiC is an ultra-hard carbide with exceptional thermal stability (decomposition temperature 3065^{o}C). It has a wide composition range which extends from 29 at% C to 50 at% C, with increasing lattice parameter with increasing C content. [42].

Fe-Cr-C and M_7C_3:

The liquidus projection of the Fe-Cr-C system indicates that primary M_7C_3 carbide is the first phase to form on cooling below liquidus temperature.[8] The residual liquid thereafter decomposes via ternary eutectic reaction into austenite and more M_7C_3 eutectic carbides.

In the past, it has been reported that large number of stacking faults are observed in the system. The possible reason for this has been reported as the reduction of the stacking fault energy of austenite by Cr [8]. It has been reported in the past that M_7C_3 has a complex hexagonal structure with a = 1.398 nm and c= 0.451 nm [8]. The resulting small c/a ratio meant that the basal plane were not closed packed and hence faulting usually occurs on the prism planes, i.e. (10.0) or (01.0) planes which are the planes perpendicular to 00.1 (basal plane). Furthermore, the occurrence of the carbide M_7C_3 in alloy steels has been the subject of many studies [43, 44, 45]. It has been suggested that the mode of formation of this carbide does in fact depend on the relative amount of Fe and Cr.

Ti-Cr-C system and Titanium and Chromium carbides:

Refractory transition metal carbides have been potential candidates for reinforcements in composite structures due to their hardness and high temperature stability. Chromium and titanium carbides have been extensively studied in terms of application for cutting tools, wear resistant linings and high wear resistance coatings. [46] Not many references were found for the Ti-Cr-C system in the literature, though the Ti-Cr [47, 48, 49], Ti-C [42, 50] and Cr-C [51, 52, 53] systems have been studied in detail. It has been shown in the past that for the Ti-Cr system, existence of a continuous series of solid solution was observed between high temperature BCC modification of β-Ti and the body centered cubic Cr. Within the Ti-C system, with a face centered NaCl structure, TiC is the most stable phase. Cr-C system indicated that the three major carbide phases present for the system are $Cr_{23}C_6$, Cr_7C_3 and Cr_3C_2. Limited investigation of the Ti-Cr-C system indicated that the solubility of TiC in chromium carbides is negligible. On the other hand, the maximum solubility of

Cr_7C_3 in TiC is ~5wt%. [54, 55] It has also been reported that no ternary phase exists in Ti-Cr-C system. [46]

It was envisioned that the background information obtained from the study of the systems based on the elements involved in the quaternary system would help in understanding the phase evolution during present laser based processing. Such background information in complement with computational thermodynamic approach is further expected to provide better control of the process parameters.

2.4 Phase Evolution: Computational Approach

Phase transitions are at the root of a great variety of processes underlying changes in composition, structure and properties of materials. Among other processes, the evolution of phases is a key fact during laser surface engineering also. The main feature distinguishing the laser from most other energy sources is the local character of action. The temporal and spatial locality of laser radiation enables one to achieve high power densities with it. Its monochromaticity provides the pre-requisite for controlling the process of absorption of radiation by matter. Hence the heating/cooling rate achieved during processing using laser as the source of energy is very high. It is for this reason that classical phase transformation theories based on thermodynamic notions of slow heat and mass transfer prove inapplicable in most cases [56]. But, these theories do give an important insight into the possible equilibrium phase transitions especially for a completely unknown system. Valuable information can be deduced from a comparative study of the possible equilibrium transitions and the non-equilibrium phases achieved during processes like laser surface engineering. The number of variables associated with

processes using laser make it impossible to experimentally verify each possible parameter. Hence, a dual approach would be employed in the current study. Firstly, with the help of computational techniques, a background of the possible reaction and phase evolution path would be developed and then some key details would be verified experimentally.

ThermoCalc™ is a computational technique to evaluate the phase diagram for different materials systems. Using thermodynamic data and phase interaction parameters of individual elements, it can predict equilibrium phases present in a binary or a multi-component thermodynamic system under the given condition. With the aid of some preliminary phase identification done using other techniques (like XRD), phase diagram for different material systems (processed using different processing techniques) can be developed relatively easily. With, the option of deliberately including and excluding phases, based on experimental observations, it is convenient to pin-point possible phases both under equilibrium as well as non-equilibrium conditions (Scheil Gulliver Model). The calculations are based on thermodynamic databases produced by an expert evaluation of experimental data. Each equilibrium calculation involves setting up and solving mathematical problem that, in ThermoCalc, involves solving a set of non-linear equations. Generating a phase diagram usually involves many such calculations.

ThermoCalc can be used to:

- Plot phase diagram (binary, ternary, isothermal) for up to 2 independent variables.
- Calculate thermodynamic properties of pure substance, compound and solution phases such as enthalpy, heat capacity and activity.
- Calculate driving force for formation of phases.

- Investigate metastable transformations such as non-equilibrium solidification simulation with the Scheil-Gulliver methods and thus know the temperature range of reactions and the reaction path.
- Perform thermodynamic calculations for different compositions within short time and thus helps in efficient and practical design of experiments.

Thus evaluation of the multicomponent system (precursor powder mixture) using this technique the software seems promising. It is known that laser processing represents non-equilibrium conditions; the results obtained using this computational techniques can help in developing good understanding of the quaternary material system used to coat the steel. Knowledge of possible equilibrium phases would help to evaluate the microstructure better.

XRD studies would be done prior to performing these calculations to have knowledge of the phases evolved after laser processing. The Scheil-Gulliver method can be employed to predict approximately the phases expected in rapid solidification. Scheil-Gulliver method is based on solidification calculation in given number of temperature steps based on assumption that there is no diffusion in solid and infinite diffusion in liquid [57, 58]. It is often useful to predict phases formed under rapid solidification. In the present work, this method would be employed to calculate solidification temperature range and the reaction path under non-equilibrium condition.

2.5 Differential Scanning Calorimetry

The objective of calorimetry is the measurement of heat which means to estimate the heat exchanged. The exchanged heat tends to effect a temperature change in a body that can

be used as a measure of the heat exchanged, or in other words, the process of heat exchange is connected with heat flow which leads to local temperature differences along its path which can serve as a measure of the flowing heat. As chemical reactions or phase transformations are accompanied by absorption or release of heat, calorimetry is a universal method for investigating such transitions.

The characteristic feature of all DSC measuring systems is the twin-type design and the direct in-difference connection of the two measuring systems which are of the same kind. The advantage of using a differential system is that temperature variations in the environment of the measuring system affect both measuring systems in the same way and hence are compensated when the difference between the individual signals is formed. The other key advantage of the DSC is that it can be heated and cooled at a preset heating or cooling rate and the transitions can be arrested during the respective cycles i.e. it is dynamic in nature.

The DSC curve offers quick information on the total measuring process. It helps in gathering precise information regarding C_p changes, thermal transitions and reactions. In addition to these usual measuring effects, it gives a quick overview of the details that if the preset temperature range was completely covered, whether disturbances of the apparatus (mechanical, electrical) occurred and whether the characteristic temperatures and peak areas lie within expected temperature ranges. Thus, the output signal from a DSC can be used to evaluate heat flow rate as a function of temperature, heat capacity change and heat of transformation for any reaction taking place within the sample.

Thus, to develop a thorough understanding of the multicomponent precursor powder mixture, it is necessary to investigate the thermal transitions taking place during

heating the powder mixture to a high temperature. The results of scan can be better interpreted by coupling the DSC results along with other structure sensitive analytical methods like X-ray diffraction, hot stage microscopy or infrared spectroscopy. So, with the help of this approach, we can develop a fundamental understanding of the temperature range, thermal stability of the carbides.

2.6 High Temperature Oxidation

AISI 1010 steel has poor oxidation resistance especially at elevated temperatures. High temperature corrosion differs from the low or room temperature corrosion. [59] This is because the rate of reaction increases by many folds at higher temperatures in the same atmosphere and hence the material degradation due to reaction with environment increases many folds with increase in temperature. Oxidation is the most important high temperature corrosion reaction, irrespective of the predominant mode in most environments.

The Ellingham diagram was referred to as the first step while investigating oxidation characteristics of any material. According to this diagram, the most stable carbides with respect to oxidation are those of Ti, Cr and Nb [59]. But one of the limitations of the Ellingham diagram is that, it does not take into account the kinetics of reaction. Hence, in addition to thermodynamic details provided by the Ellingham diagram, the material system needed to be kinetically investigated to comprehend the rate of reaction. The different laws commonly encountered during oxidation kinetic investigations are logarithmic (direct and inverse), parabolic, linear or a combination of these. Among these, logarithmic laws generally apply to the low temperature thin layer

regime. The linear law is applicable to systems where oxidation remains constant with time and is generally the most undesired one. The equation governing this law is

$$\frac{dw}{dt} = kt$$

Parabolic oxidation rate laws are of great importance with most engineering alloys. As per this law, oxide growth occurs with a continuously decreasing oxidation rate. The rate of occurring reaction is therefore inversely proportional to the scale thickness or the weight of oxide formed.

$$\frac{dw}{dt} \propto \frac{1}{w}$$

where w represents the weight of oxide formed per unit area exposed. Integrating,

$$w^2 = 2kt + c$$

where k and c are oxidation constants. In general, the law governing the oxidation kinetics is a combination of these laws.

During oxidation investigation, the details needed to obtain a viable model of the oxidation process are data on kinetics of reaction, characterization of the formed product and information on the structure of interface between the oxide and the metal or alloy is required. Among these, the most important data needed are the kinetics and rate law for the oxidation process [59]. The current study, on the oxidation behavior of the coating, laid stress on this aspect. Thermogravimetric techniques were employed to investigate the oxidation kinetics of the coating. Thermogravimetry is the measurement of mass change (for a known exposed area) with increasing temperature or time at constant temperature.

The latter is usually used for oxidation studies while the former is employed for chemical or decomposition reactions.

2.7 Flow Diagram

A brief flow diagram of the study is presented in Fig.1. Following a methodical approach, an effort was made to formulate and characterize the laser *in-situ* synthesis of carbide coatings within the surface layers of steel.

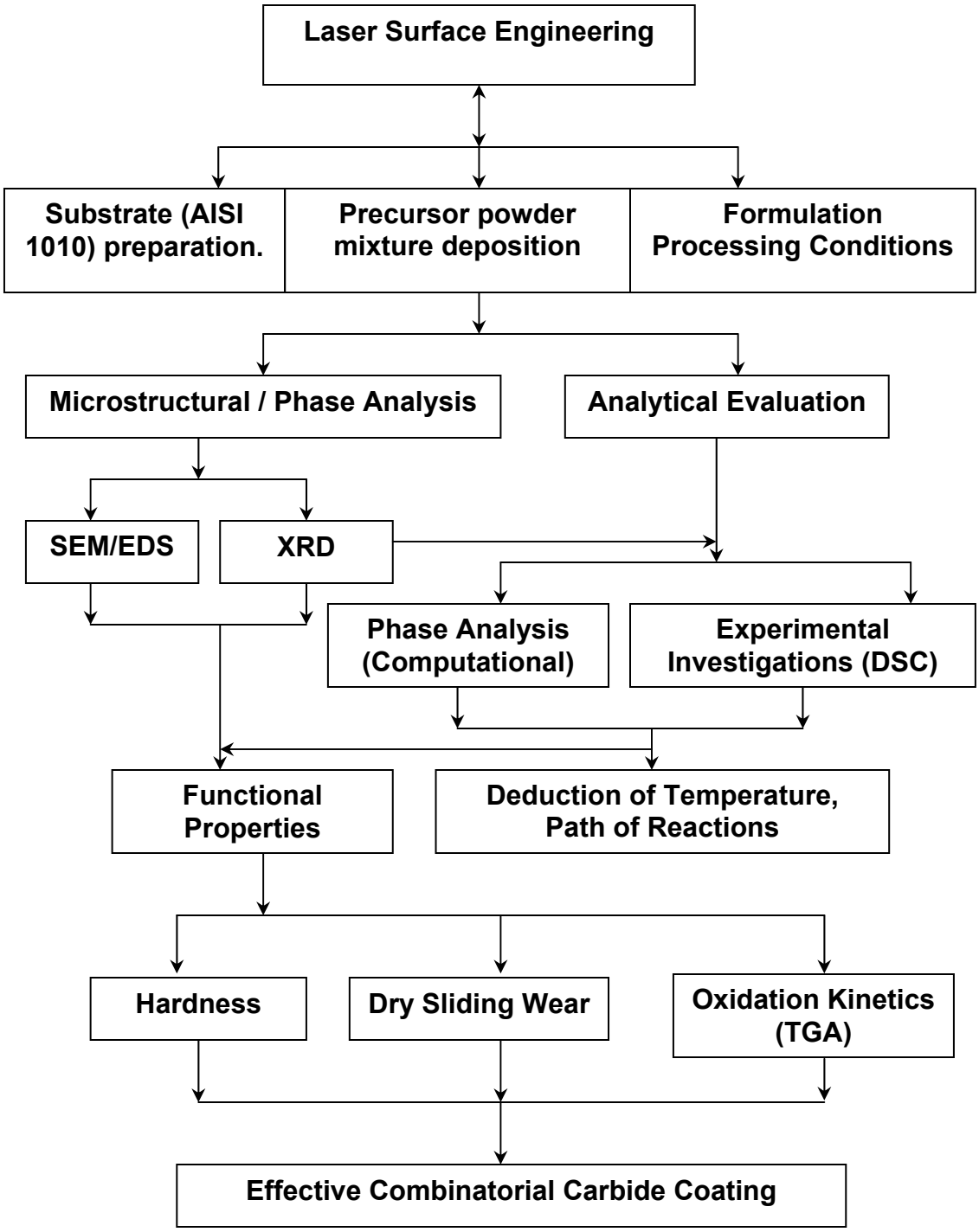

Figure 1: Flow diagram of the investigation

Chapter 3

3. EXPERIMENTAL PROCEDURE

3.1 Laser Processing

AISI 1010 steel (low carbon steel with a nominal 0.10 wt% C) was used as the substrate material in the present study, with the coating being an Fe- based alloy containing Ti, Cr and C. Rectangular plates (7.5 cm x 5cm x 0.5cm) of the substrate were sand blasted followed by washing with acetone and methanol to provide a clean and consistent surface. A mixture of commercially available Fe (99.9% pure), Ti (99.5% pure), C (99.5% pure) (all having average particle size < 45μm) and Cr (99.8% pure, average particle size 10 micron or less) powders, supplied by CERAC, Milwaukee WI, were used as a precursor material. 20 wt% Ti, 20 wt% Cr, 5 wt% C and rest Fe powder were blended together and suspended in a water soluble organic binder to form a thick slurry. The slurry of precursor material was air spray deposited on the substrate for uniform green (unprocessed) thickness and then dried at 75^{o} C for 30 minutes.

A 2.5 KW Hobart continuous wave Nd: YAG laser equipped with a fiber optic beam delivery system was employed for laser surface engineering. Fig. 2 depicts a schematic outline of the steps involved during laser processing of the as- received AISI 1010 steel sample. Parallel tracks with partial overlapping (~15%) were laid with the laser beam focused 0.5 mm above the surface of the substrate. A range of different beam powers was used over a set of samples keeping the laser scan speed constant to 1500 mm/min. Argon was used as cover gas. The nozzle and working distance was kept

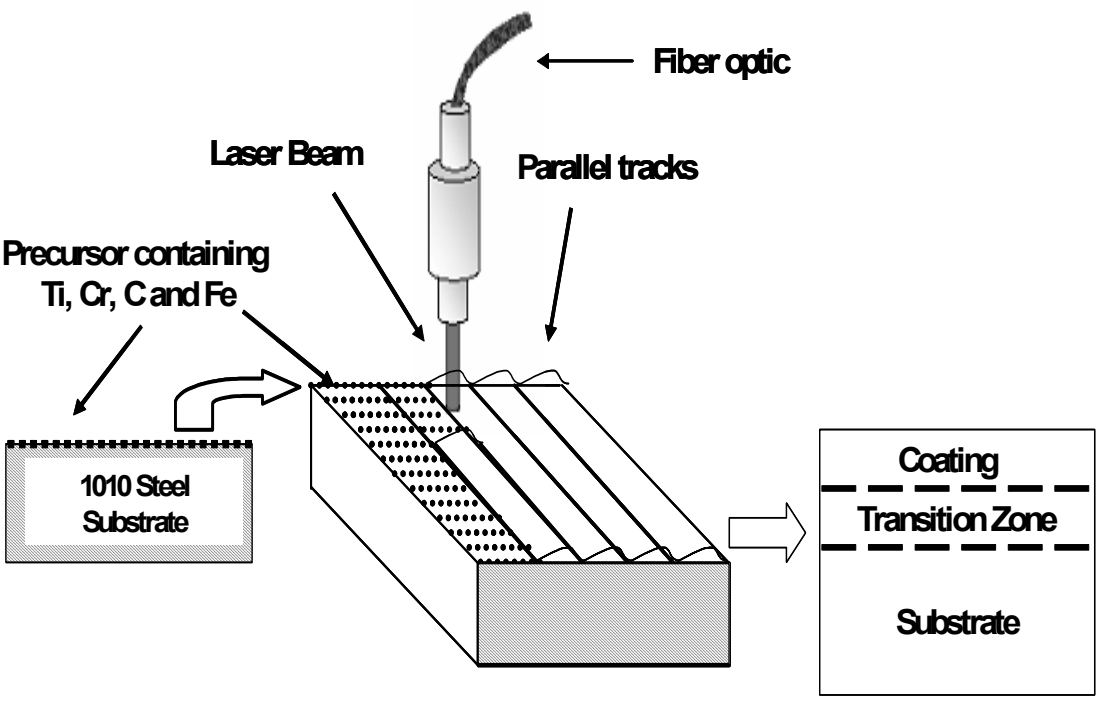

Figure 2: Process schematic depicting the steps involved in the process.

Table 3: Processing parameters used for laser treatment.

Sample	A	B	C	D	E
Power (W)	900	1300	1500	1900	2100
Energy Density (W/cm^2) x 10^4	5	7.2	8.3	10.5	11.6
Scan Velocity (cm/min)	150	150	150	150	150

constant at 20mm to 132 mm respectively for all the processing powers. Table 3 lists the processing parameters used for the study. The fiber optic beam delivery system consisted of the input coupling g module, the fiber optic and the output coupling module. The input coupling module focuses the laser output onto the end of the fiber. The optical fiber in the present system is 16 m long and about 600 μm in diameter. The output coupling module is a telescopic tube (6.32 cm diameter) that can be housed with various configurations of cylindrical and concave lenses firstly to collimate and then either to focus or defocus into various shapes of the beam onto the work-piece. In the present study, in order to provide a large sweeping coverage (i.e. rapid processing speed) and to reduce and/or to eliminate overlap between the successive laser passes, lenses within the output coupling module were configured to provide a beam of 2.5 mm wide line in spatial distribution onto the sample surface. Such compact and rugged design of the output-coupling module on the optical fiber provided a higher degree of flexibility and access during laser surface processing.

3.2 Characterization

The characterization of the coating was done by using optical microscopy, scanning electron microscopy, energy dispersive spectroscopy (SEM/EDS) and X-ray diffractometery (XRD).

3.2.1 Microstructural Characterization

Samples were sectioned perpendicular to the laser processing direction and mounted in bakelite. The cross-section of the laser treated sample was polished using 400, 600, 800 and 1200 grit SiC pads (supplied by Buehler) and then alumina slurry on a microcloth. Microstructural investigation of the polished and etched samples was done on a Hitachi S3500 SEM. The samples were over etched so that the fine microstructure achieved during laser processing can be revealed and a sharp contrast between the carbide particles and the matrix can be obtained. Energy dispersive spectroscopy (EDS) of the polished and etched samples was done to identify the particles observed within the coating in the SEM images. EDS was done at low voltages in an attempt to investigate the presence of low atomic number element (C) in *in-situ* grown particles with the aim of identifying carbide particles.

3.2.2 Structural Characterization

X ray diffraction studies of the coating were conducted to identify and characterize the various phases present in the laser modified surface region. Attempts were made to make a coating of around 200 micron depth. Due to the laser treatment at high powers, part of

the substrate, along with the pre-placed powders, is melted, mixed and solidified. The reaction which takes place in the melt pool is arrested as the solidified phase due to the rapid nature of the process. Hence, the XRD studies of the samples would help in comprehending the phases formed because of reactions during laser processing. A Phillips Norelco X-ray diffractometer with Cu K_{∞} radiation (1.54Å), operated at 40 kV and 20 mA, was used for this. Samples were sectioned perpendicular to the coating into small pieces (1.5cm x 1cm x 0.5cm). The specimen was scanned at a step size of 0.02 deg and for a count time of 1s with diffraction angles varying between 20 and 100 degrees. Structural characterization was done for the whole set of processing conditions twice to confirm the presence of the phases.

3.3 Computational Thermodynamic Calculations

It was practically impossible to conduct experiments which can map the entire set of processing variables. With a matrix of processing powers used for laser treatment of the surface, it is necessary to develop a model to understand the effect of variation in processing conditions and comprehend the best possible parameters. Thus, computational techniques were employed to understand the reasons for phase evolution. The windows based version of ThermoCalc™ software (TCW 2, version 2.1.0, © Foundation for Computational Thermodynamics, Stockholm, Sweden) was used to perform thermodynamic calculations for the current multicomponent alloy system. The TC Fe2 database (TC Fe2 Thermo Calc Steel Database v.2) was used for the calculations. The calculations were done for a set of different variables. Calculations were also performed using the Scheil module of the software (which is based on conditions similar to those in

non-equilibrium processing) to evaluate the temperature range of phase transitions. Quantitative estimation of the evolved phases with variation in the amount of particular elements in the precursor mixture was done. Computational investigation of the stability of the phases with temperature was done to gauge the thermal stability of the phases. Analytical evaluation of the thermal stability and temperature range of reactions were done later (using DSC) to confirm the results obtained by computational techniques.

3.4 Differential Scanning Calorimetry

Although the heating/cooling rates attained during LSE can be far different than that are available for DSC runs, the perception behind the current effort was that a fundamental understanding of the coating alloy mixture. Table 4 briefly mentions the sample

Table 4: Sample specifications and conditions used during DSC.

Sample No.	Sample specifications	Conditions
1	Fe,Ti,Cr,C (powders)	Heating: 40 K/min from 25 to 1175 ^{o}C, Cooling at 40 K/min.
2	Fe,Ti,Cr,C (1)	Rerun (1):- Heating: 40 K/min from 25 to 1175 ^{o}C, Cooling at 40 K/min.
3	Ti, Cr, C (powders)	Same conditions as 1
4	Fe (powder)	Same conditions as 1
5	Fe,Ti,Cr,C (laser processed coating)	Heating: 40 K/min from 25 to 1525^{o}C and cooling back at rate of 40 K/min.

specification and the conditions in which DSC studies were performed. First set of samples consisted of a mixture of commercially available Fe (99.9% pure), Ti (99.5% pure), C (99.5% pure) (all having average particle size <45micron) and Cr (99.8% pure, average particle size <10 microns or less) powders, supplied by CERAC, Milwaukee WI. The powder mixture contained 20wt% Ti, 20wt% Cr, 5wt %C and rest Fe (same composition used as precursor). DSC runs were done on the powder mixture in a Netzsch 404 (Paoli, PA) high temperature differential scanning calorimeter (HTDSC). Sapphire was used as the reference material. The weighed quantity of the powder mixture was heated in an alumina crucible. Prior to the experiments, the DSC cell was purged with argon and the heating and cooling were done under constant argon flow. The presence of Ti and Fe made purging with argon imperative as both of them are highly susceptible to oxidation. DSC runs (heating and cooling) were done on the elemental powder mixture heated at a rate of 40 K/min from 25^{o}C to 1175^{o}C and immediately back to 25^{o}C. The same sample was then reheated at the same heating rate to the same temperature to investigate any reversibility of reactions or decomposition of the reaction products. DSC runs were also performed on powder mixture of Ti, Cr, C (4:4:1 wt%) and on pure Fe powders. These runs were done to interpret the results of the runs done on the first sample.

The second set of samples consisted of laser-treated samples processed at 1500 W. The resulting coating was shaved off the processed sample using a Buehler Isomet low speed saw. A part of this coating was used for DSC runs and heated at 40 K/min from 25^{o}C to 1525^{o}C. The 40 K/min rate was chosen as it was the limit of controlled

cooling rate of the DSC machine. The highest rate available with the DSC was chosen because the conditions during laser processing provide rapid heating rates.

XRD analysis was conducted for heated powder samples on a Philips Analytical B.V. instrument to identify and characterize the various phases evolved during DSC runs. The diffraction studies were done between 20 and 90 degrees. Since the amount of powder used in DSC runs was very small and 4 different elements involved, the XRD runs resulted in spectra with a lot of noisy background. In an attempt to unravel this problem, two steps were taken. Firstly, the continuous scans were done at a very slow rate with a step size of 0.02 degree and 4 seconds time per step. Secondly, appreciable amount of powders, heated and cooled under the identical conditions in an Infrared furnace, were procured. The flowchart of the heating and cooling cycle, in the furnace, is presented in the Fig. 3.

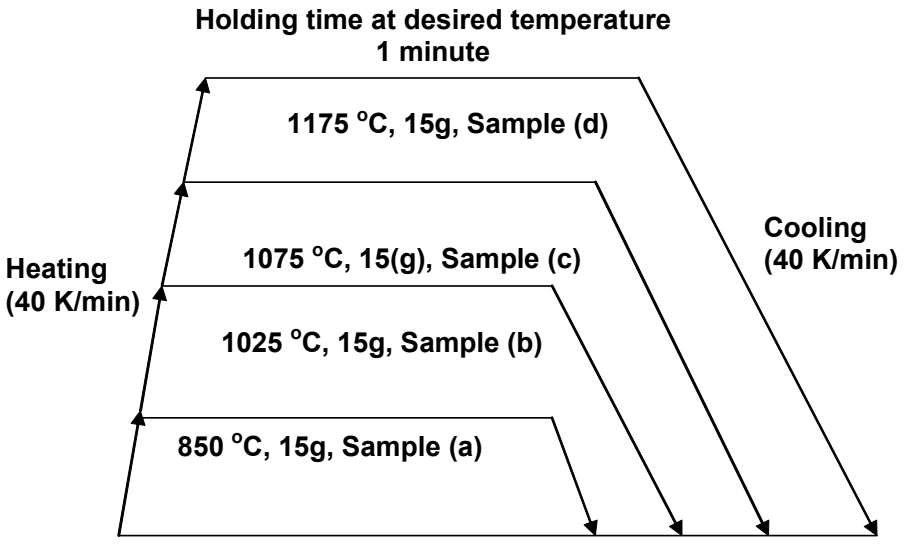

Figure 3: Schematic of the heating process in the Infrared furnace.

Furnace heating for all powders was carried out in an alumina-zirconia crucible. 15g of powder in a crucible was loaded into the Infrared furnace and a thermocouple was placed in the powder. Vacuum was pulled to 200mTorr and the furnace was backfilled with Ar to -5psi. The backfilling procedure was performed successively for three times followed by creation of vacuum of 200mTorr.The powders were heated at 4 different temperatures identified by the thermal events during DSC runs at 850, 1025, 1075, and 1175^{o}C with the same rate as in DSC runs. Thereafter, XRD analysis for the arrested phases was done for all the samples.

3.5 Functional Properties

The functional properties have been characterized for hardness, wear and high temperature oxidation.

3.5.1 Microhardness Results

Due to the rapid rate of laser processing, the interaction of the laser beam with the substrate and the precursor powder takes place to a certain depth only. Due to these reactions in the surface layers, it was expected that some change in the hardness of the samples would be seen and hence needed to be investigated. Cross-section of samples polished in the way described earlier was subjected to microhardness test. Microhardness measurement was performed on a LECO microhardness tester LM 300AT with a Knoop indenter. A normal load of 100g was applied for 15s during the test. Indentations were made across the coating into the substrate at an interval of 50 μm. Comparative plots of

the results for various samples were plotted thereafter to understand the effect of processing parameters on the microhardness of the coating.

3.5.2 Wear Studies

Dry sliding wear tests were performed on in-house built block-on-disk equipment. The tests were conducted on both substrate and coated samples. The weight loss during wear is an indication of the wear resistance of the sample i.e. the lower the weight loss, more wear resistant the material. A normal load of 5.2 kgf was applied during the test. The wheel used to wear the samples was 4130 HT steel (65 Rc). It was translated at 44 ms^{-1} linear speed and weight of the samples was noted at every 2 minute interval for a total period of 10 minutes to estimate the loss of material due to wear. Plots of cumulative weight loss vs. time were plotted thereafter to comprehend the comparative weight loss for different samples.

3.5.3 High Temperature Oxidation Analysis

Oxidation kinetic studies were carried out using a Mettler Toledo Thermogravimetric Analyzer (TGA/SDTA851e). Oxidation tests were conducted at 700 and 1000 ^{o}C for samples processed at laser powers ranging from 1300-2100 W. The TGA furnace for operated by increasing the temperature from 50-700 ^{o}C and 50-1000 ^{o}C at 10 ^{o}C/min respectively. The samples were held at the test temperatures for 180 minutes, after these temperatures were attained. Thereafter, the samples were cooled at a fixed rate of 10^{o}C/min thereafter. All the experiments were conducted in a constant flow of commercial grade bottled breathing air. The samples were prepared by shaving the coating of the laser processed sample using an Electrical Discharge Machine (EDM) to a

thickness of 500 micron. Thereafter, the thin slices were polished from the substrate side on abrasive papers to ensure that the sample consisted of only the coating and does not have substrate, which could influence the oxidation behavior of the composite coating. This was accomplished by estimating the thickness of the coating for samples processed at various powers using the SEM/EDS. Continuous plots of weight gain per unit area vs. time for which the sample was held were used for predicting oxidation kinetics of the samples.

Chapter 4

4. RESULTS AND DISCUSSION

The results obtained during experiments done for characterization of the coatings are presented in this chapter. Following a step by step procedure, an effort was made to develop a thorough understanding of laser assisted surface modification of the commonly available steel with the quaternary coating system.

4.1 Microstructural Evolution

As shown schematically in Fig. 2, due to interaction with the laser beam, the surface of the as-received sample (pre-deposited with a precursor elementary powder mixture) was modified to form three zones. These include the coating, transition zone and the substrate. These zones have a distinct interface between each other and the microstructure varies gradually through the three zones. The thickness of the coating region is 200-225 microns, with minor variations in regions where laser tracks overlap. The scanning electron micrograph of the cross section of the steel sample after laser surface treatment is illustrated in Fig. 4a. The sample was over etched with 5% nital to get a sharp contrast between carbide particles and matrix during SEM analysis. A uniform, adherent, crack free and metallurgically bonded coating along with the heat-affected zone and the as-received substrate material is depicted in the figure. The substrate AISI 1010 steel has a nominal 0.10 wt% C and consists mainly of coarse grains of ferrite with few lamellae of pearlite within intergranular regions. During laser processing, the interaction of laser with substrate is only up to a limited depth, due to the very high speed involved in the process

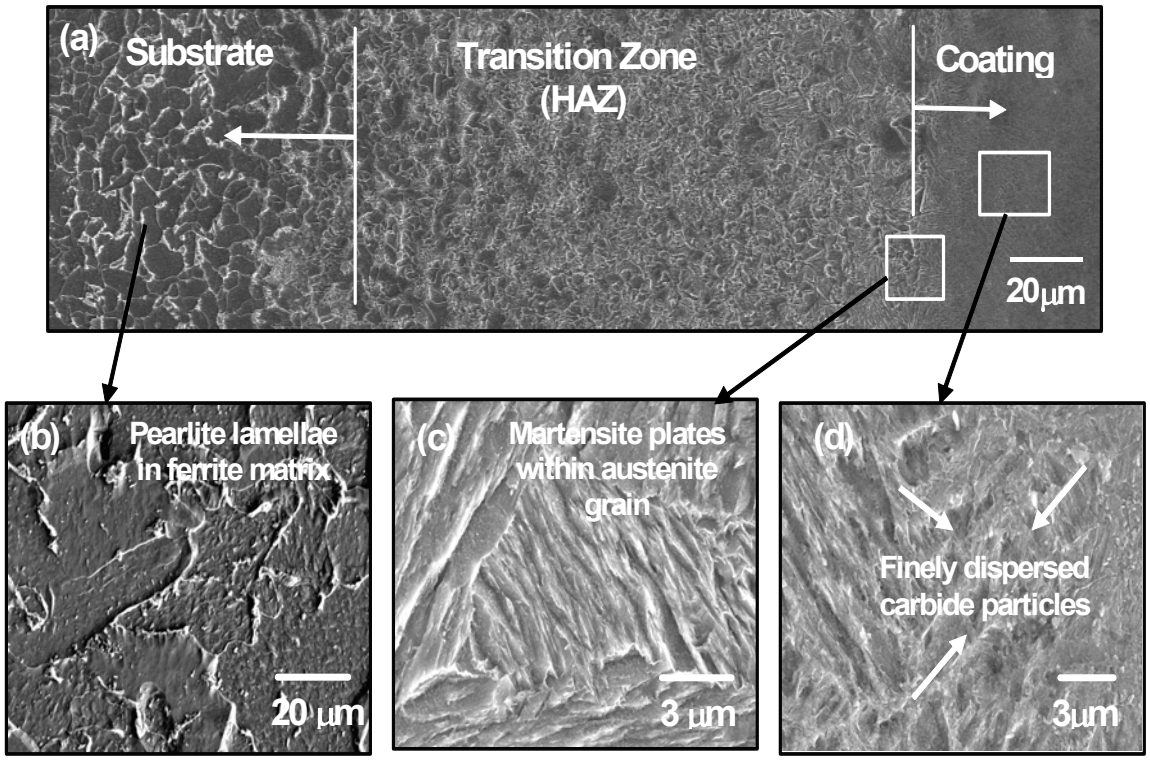

Figure 4: Scanning electron micrograph of sample processed at 1500 W (a) higher magnification overview of the cross-section and image of (b) substrate, (c) transition zone and (d) coating region.

and hence the substrate remains unaffected below a certain depth (approximately 350μm) (Fig. 4b). The heat affected zone (HAZ) is a transition region between the coating and the unaffected base material. In a higher magnification image (Fig. 4c), HAZ consisting of martensite plates having different orientations and the habit plane (the preferred crystal plane of austenite on which martensite crystal forms) is shown. This heat-affected zone has a distinctly sharp interface with the coating region (Fig. 4a).

Within the coating, uniformly distributed *in-situ* formed carbide particles are observed (Fig. 4d). Martensite plates observed both in the HAZ and the coating was expected due to the very high cooling rates associated with laser processing of materials. X-ray diffraction analysis (XRD) (discussed later) further confirmed the presence of characteristic peaks of martensite and carbides in the coating. A large refinement of grains along with in-situ formation of carbides during processing is expected to lead to improvement in strength and hardness of the steel.

Further details of the coating have been depicted in SEM images of the coating region of the sample processed at 1500W. The carbide particles are uniformly distributed throughout the coating (Fig. 5). It has been reported in the past that residual pores and agglomeration of TiC particles in a ferrous matrix has been observed in composite layers formed by different processes, which necessitates the use of flux (MgO-CaO) to avoid it.[60] However, in the present study, no porosity was observed within the coating or on the interface with the substrate.

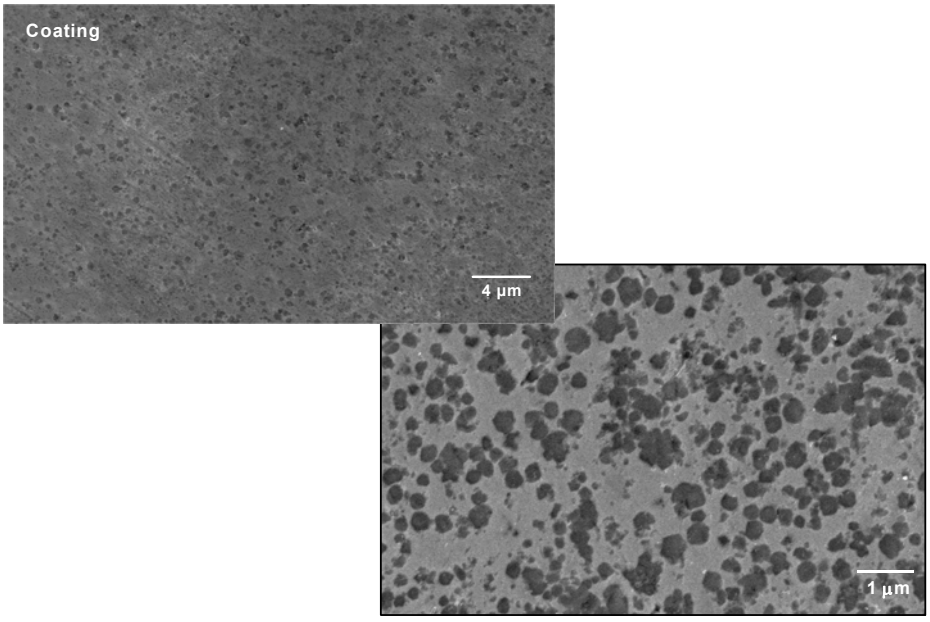

Figure 5: Scanning electron micrographs of the coating (surface composite layer) indicating uniform distribution of in-situ grown particles.

A higher magnification image of the coating is shown in Fig. 6(a). The samples were heavily etched with nital to reveal the details. Since the TiC particles are inert to this etchant, preferential etching around the edges of the carbide particles is observed in the ferrous matrix and as a result, the distinct shape of the carbide particles is visible. The average size of the particles, estimated from the micrograph, is approximately between 200-400 nm. The ultra fine size of the particles makes distinct compositional mapping using energy dispersive spectroscopy (EDS) difficult. But, the EDS results still gave a relative approximation of the elemental composition of a small area. It is understood that further analysis using other techniques like Transmission Electron Microscopy (TEM) studies are necessary to confirm these observations.

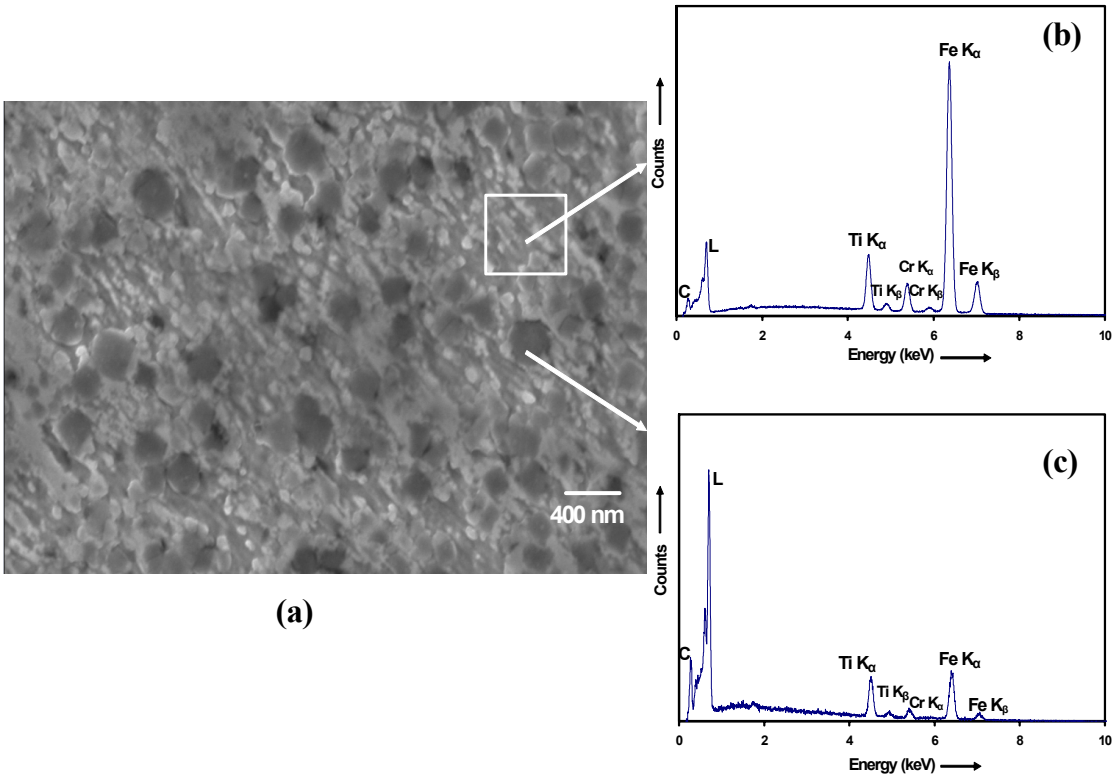

Figure 6: SEM image of the coating (1500 W) (a) Higher magnification view and, EDS of (b) the matrix and (c) black particle.

Similar microstructural features were observed for all other samples processed under different powers (900, 1300, 1900 and 2100 W) and hence individual images of all samples have not been presented here. Attempts were made to conduct EDS compositional map analysis (Fig. 6b and 6c) corresponding to the matrix and the particle respectively from Fig. 6a. The peak marked L represents the L lines for the elements Fe, Ti and Cr. Since these lines are so close, they overlap each other to form a very broad peak. The EDS had to be done at a relatively low voltage (due to the presence of low atomic number element like C) and hence the presence of L lines was expected. The other major peaks present in Fig. 6b are Ti, Cr, Fe (both K_α and K_β for all the three) and C. In Fig. 6c, the relative amount of Ti with respect to the other elements is higher than that in the matrix (Fig. 6b) which indicates that the particle is richer in Ti. As mentioned earlier, since the particle size is too small, the EDS found peaks for other elements also. Both Kα and Kβ peaks for Ti and Fe exist while only Kα peak exists for Cr (Fig. 6c). In comparison to the black particle (in Fig. 6a), EDS results for surrounding matrix, indicated higher Cr and Fe content (Fig. 6b). Comparison of these two spectra confirmed that the black particles are TiC particles, which precipitate out by the reaction between Ti and C in the melt pool. These particles are uniformly dispersed in a ferrous matrix.

Ti has very strong carbide forming tendency reacts with C to form TiC. [61] The rate of formation of nuclei in a melt is given by the following equation [62]

$$I = K_1 \exp(-K_2 / T\Delta T^2)$$

where K_1 and K_2 are constants, ΔT is the undercooling and T is the temperature of the liquid. Since, during the formation of TiC, molten Ti flows to the solid C particles and reacts to form TiC [63], hence the equation is applicable to formation of the carbide. As

ΔT increases, the formation of large number of small nuclei of critical size takes place. Since the ΔT term is in the exponential, it has a profound effect on the rate of nuclei formation. A very high undercooling is associated with laser processing and hence as TiC precipitates out of the molten pool, large number of TiC nuclei formation is observed. The rapid speed of the process and the rate of solidification associated with laser processing do not give the particles enough time to grow forcing them to retain their fine sizes. Hence, very fine TiC particles are observed in the surface modified layer of the processed samples (Fig. 5 and Fig. 6a). Composites reinforced with fine particles are expected to possess more wear resistance in comparison to coarse particles reinforcements. This higher wear resistance can be attributed to better matching of carbide particles with the matrix and the decreased mean free path of the composite. [2]

The particles are seen to be uniformly distributed within the coating (Fig.5). The problem of inhomogeneous distribution of TiC (or many other ceramic particles used as reinforcing phase in a composite) is confronted during fabrication by electron beam irradiation [60]. The unmelted TiC generally tend to float in the liquid melt pool. Conversely, in the current process, uniform distribution of TiC particles was observed due to their *in-situ* growth from the melt pool. The heat convection in the melt pool during the process helps in performing a stirring action and hence their limited growth (into ultra fine size) and uniform distribution in the coating. In addition to the hardness and size of the reinforcing phase, the matrix hardness also plays an important role in improving the abrasion resistance. The supporting ability of the matrix improves if a martensitic matrix exists rather than retained austenite [64]. The presence of martensite in

the coating has been corroborated by the diffraction spectra for the laser-processed samples (discussed in the next section).

Another important factor that plays a role in the formation of this ultra fine particle composite layer is the refractory nature of the carbide. As mentioned in the introduction (Chapter 1), the two difficulties associated in forming a nanostructured material is grain growth and sliding and one way to avoid this is the introduction of a hard phase. TiC being refractory carbide is thermally stable until very high temperatures (decomposition temperature of 3065^{o}C). The typical temperature at which grain growth takes place is higher than 0.5 times the melting point of a material. The refractory transition metal carbides have a high melting temperature and a lower diffusion coefficient. Hence, the growth of this partially ionic-covalent bonded TiC is not possible until very high temperatures and much higher driving force (in terms of thermal energy, chemical energy or stress) is required to make the growth of TiC particles possible. Thus the ultra fine TiC particles are stable and remain an active reinforcement. These carbide particles maintain their sizes during application and hence the surface modified steel can retain its tribological properties till very high temperatures and under severe conditions. The thermal stability of the carbides was verified experimentally using DSC and has been discussed in detail in section 4.3.2. The results of wear studies and high temperature oxidation have been discussed later in section 4.4.2 and 4.4.3 respectively.

Very fine white particles were observed in the matrix in addition to the black particles. These particles could be broken dendrites which are evenly distributed due to the heat convection in the melt pool. During laser processing, the beam traverses over the surface at very high speeds thus interacting with the surface just for an extremely short

duration (<seconds). Melting takes place only for a short time in a confined near-surface volume and bulk of the material remains cooler and thus forms a heat sink. The rate at which growth of a particle occurs depends on the cooling rate associated with the process. Preliminary calculations for temperature and cooling rates associated with the laser processing of samples was done using a two color optical pyrometer which indicated cooling rates of the order of 10^3 K/s. The general cooling rate associated with laser processing of Fe based alloys is of the order of 10^{3-7} K/s [65].

Additionally, these observations were confirmed by XRD studies. XRD analysis was intended for identification and confirmation of additional phases present in the laser modified region of all samples processed under different laser powers (900-2100W).

4.2 Phase-Structure Dependence on Laser Processing Power

XRD analysis provided the presence and identification of various phases in surface and subsurface regions of laser processed samples. This included TiC, Fe-Cr, M_7C_3, α' (martensite) and γ (austenite) (Fig. 7). Furthermore, based on the XRD analysis, a distinct pattern for the type of phase formation, as a function of laser power was noticed and accordingly it is divided into 2 groups. The first group of samples possessed the phases TiC, Fe-Cr, M_7C_3, α' and γ while the second group of samples possessed TiC, Fe-Cr, α'. The spectra of the two groups have been designated as Group 1 for samples processed at 900, 1500 and 2100 W and Group 2 for 1300 and 1900 W respectively. For convenience, from here on, the samples of Group 1 would be referred to as A1, A2 and A3 and those of Group 2 as B1 and B2 respectively. Since Ti is a very strong carbide former, as expected, all the samples show prominent peaks of TiC thus confirming *in-situ* formation of

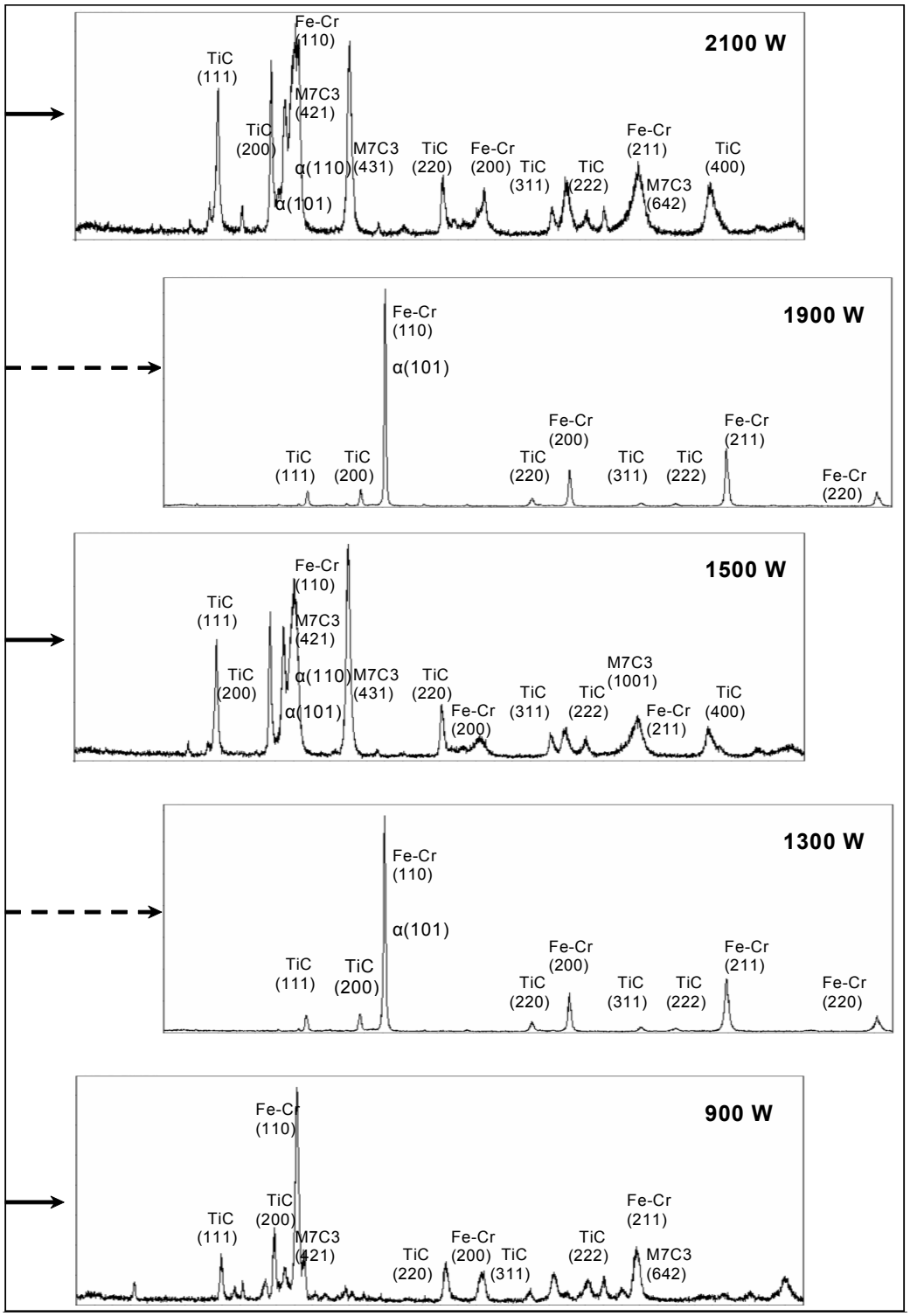

Figure 7: X ray Diffraction spectra for samples processed at different laser powers.

TiC. In addition to this, the intensity of TiC peak increases with the beam power used for laser processing. The various phases present in the spectra, their crystal structures along with the space groups and lattice parameters are enlisted in Table 5. Another phase, ferrite Fe-Cr (α), a substitutional solid solution of Cr in Fe is prominently present in all the samples. It is well known that Cr is a ferrite stabilizer [39] and helps in improving the strength and toughness of ferrite in steels. Also, according to Hume Rothery laws [39], the range of solubility in solid solution can be determined by (a) Chemical structure factor (b) Relative size factor (c) Chemical affinity factor (d) Relative valence factor. The crystal structure of both Cr and Fe is bcc as is the structure of Fe-Cr (as suggested by the space group of Fe-Cr mentioned in Table 5). The relative size factor implies that if the difference in the atomic radii of the two elements involved is less than about 15%, the chances of formation of solid solution is high. The difference between the atomic radii of Fe and Cr is 0.4% as the atomic radii of Cr and Fe is 2.49 Å and 2.48 Å respectively. The chemical affinity of elements increases depending on how far they are separated in the periodic table; Fe and Cr are separated only by one element and hence they have low chemical affinity. The chance of forming solid solution increases with decrease in chemical affinity. The relative valence factor suggests that a metal with a lower valence tends to dissolve a metal with higher valence more than vice versa. Fe has a lower valence than Cr and hence tends to dissolve it more. Thus, the formation of Fe-Cr phase as a result of the laser processing can be comprehended.

The spectra of samples A1, A2 and A3 indicated the presence of a phase M_7C_3 (M= Cr, Fe), which is a complex carbide of a hexagonal close packed structure and has a lattice parameters of c = 4.52Å and a= 13.98 Å. The formation of such complex

Table 5: List of various phases identified during XRD.

Phase	Crystal Structure	Space Group	Lattice parameter	Samples in which present
TiC	Cubic	Fm3m	a = 4.33 Å	A1,A2,A3, B1,B2
Fe-Cr	Cubic	Im3m	a = 2.88 Å	A1,A2,A3, B1,B2
M_7C_3	Hexagonal close packed	P31c	a = 13.98 Å c = 4.52 Å	A1,A2,A3
Martensite (α`)	Tetragonal	I4/mmm	a = 2.86 Å c = 2.96 Å	B1,B2,A2,A3
Austenite (γ)	Cubic	Fm3m	a = 3.60 Å	A2,A3

chromium carbide can be attributed to the high concentration of Cr in the precursor coating and to the rapid cooling rate associated with laser processing. Also, in the case of Fe-Ti-C system, TiC formation occurs with Ti depletion in the system that could lead to the tendency of Fe to form cementite.

But, since a high percentage of Cr (20 wt%) was present in the precursor alloy, formation of M_7C_3 type carbides took place in preference to the Fe_3C as Cr has a higher tendency to form carbides than iron. The various reaction equations, accompanied by their respective free energy changes for the formation of carbides from respective elemental state, have been listed in Table 6 [66]. The free energy values help in predicting the formation of carbides relative to each other. As indicated in Fig. 8 for the free energy of formation of the carbides with respect to temperature, Ti and Cr have stronger carbide forming tendency than Fe. (The free energy values are much lower for both TiC and Cr_7C_3 than Fe_3C).

Table 6: Free energy of reaction as function of temperature.

Reaction	Free Energy (J/ mole)	Temperature Range(^{o}K)
(1) Ti + C = TiC	-183172 + 10.09 T	298 – 1155
	-186731 + 13.2 T	1155 – 2000
(2) 7Cr + 3C = Cr_7C_3	-174401 – 25.9 T	298 – 2171
	-360902 +60.08 T	2171 – 2938
(3) 3Fe + C = Fe_3C	25958 – 23.27 T	298 – 463
	26711 – 24.78 T	463 – 1115
	10362 – 10.17 T	1115 – 1808

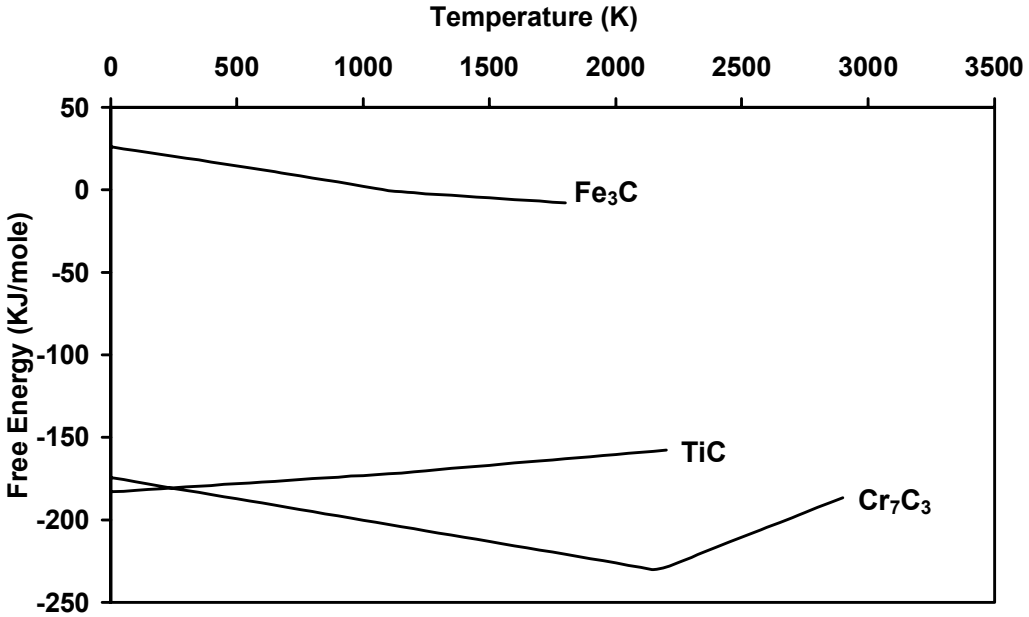

Figure 8: Variation of free energy of carbides with temperature.

Values for the Cr_7C_3 phase were chosen instead of M_7C_3 as fixed values for free energy of formation for this phase (M_7C_3) were not available and Cr_7C_3 was the closest match. Interestingly, the free energy value for Cr_7C_3 is much lower than TiC for most of the temperature range (298-2000K). However, on the contrary, the experimental observations indicated TiC as prominently present in all the samples (Table 5) and absence of Cr_7C_3 in samples B1 and B2. In view of this, it can be postulated that as the tabulated free energy values are for pure elements, the presence of both Ti and Cr would affect the activity of each of them. This hypothesis (presence of other elements effects the activity of each) was experimentally confirmed later with DSC experiments (discussed in Section 4.3.2). This might influence the type of carbides formed. Also, this corroborates the fact that LSE is a non equilibrium process and formation of metastable phases can take place as a result of the rapid speed of the process.

While the high cooling rates in the laser processing of materials formed metastable phases like martensite (A2, A3, B1 and B2 in Fig. 7), the presence of retained austenite peaks (in samples A2 and A3) can be attributed to the fact that 5 wt% C was added in the precursor and C being a very strong austenite stabilizer, reduces the M_s (Martensite start) temperature considerably. The absence of both retained austenite and martensite in the sample A1 (Fig. 7) is probably due to lower power of processing (900 W) and hence lower temperature of the substrate, leading to a lower cooling rate. The essential difference between the Group 1 (A1, A2 and A3) and Group 2 (B1 and B2) is the presence of Cr-carbides in the former and its absence in the latter, although TiC is prominently present in all samples. At the powers used for processing samples in Group 2 (1300 and 1900 W), the entire chromium appeared to have gone into a solid solution with

Fe to form Fe-Cr thereby preventing the formation of Cr-carbides. An approximate estimate of this solid solution present in respective samples is ascertained by calculating the ratio of integrated intensity of Fe-Cr (α) peaks to integrated intensity of the entire spectrum of the sample (Table 7). The quantitative analysis is based on the fact that the intensity of the diffraction pattern of any specific phase in a mixture of phases is dependent on the concentration of that phase in the mixture [67]. This ratio is higher in samples B1 and B2 (> 0.85) than in samples A1, A2 and A3 (< 0.40).

To summarize the XRD results, a schematic of the phases evolved with respect to power is depicted in Fig. 9. The key fact to note is the presence of the chromium carbide phase (M_7C_3) in the coating. This phase oscillates between different processing conditions (with increasing processing power) i.e. it is present within the coating for certain intermediate processing conditions (solid arrows for 900, 1500 and 2100 W) and absent for the remaining (dashed arrows for 1300 and 1900 W) in Fig. 7. This behavior was verified by processing the samples multiple times under similar conditions.

Table 7: Ratio representing an approximate estimate of the relative amount of Fe-Cr present in samples processed at various powers.

Processing Power (Sample)	Estimated amount of Fe-Cr
900 W (A1)	0.388
1300 W (B1)	0.859
1500 W (A2)	0.092
1900 W (B2)	0.871
2100 W (A3)	0.239

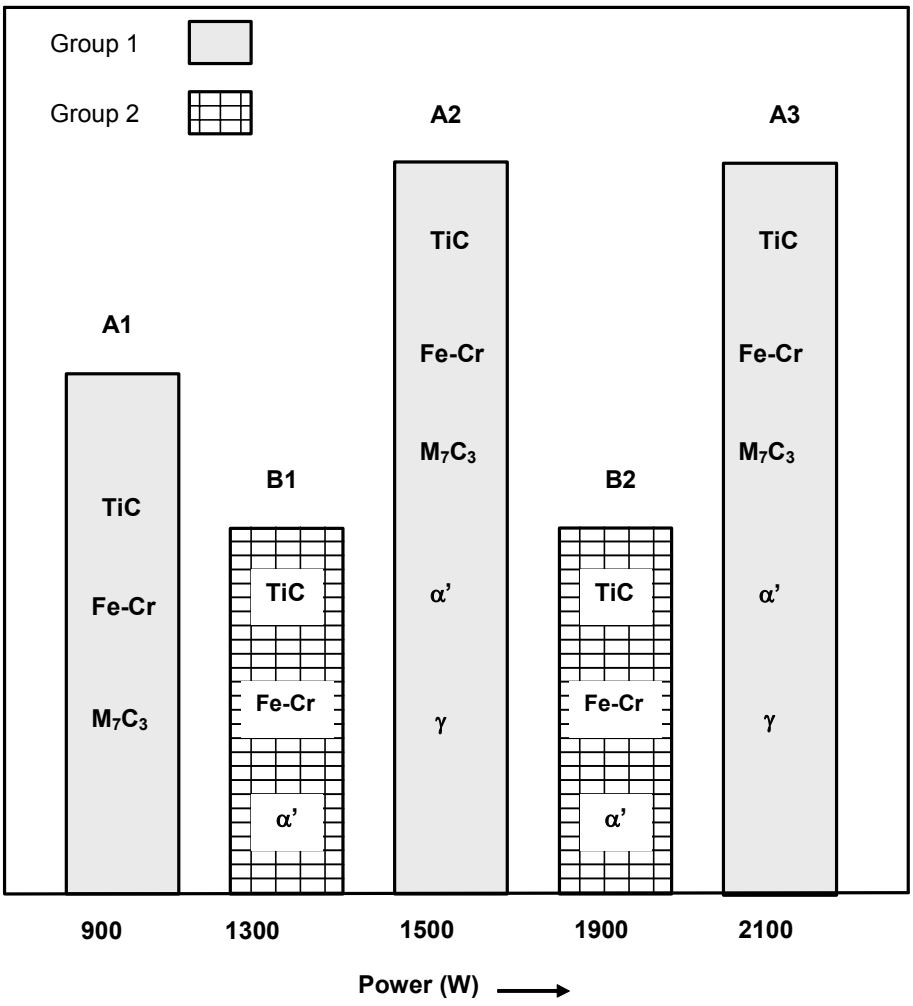

Figure 9: Schematic of reaction products as a function of laser processing power.

The results obtained thus far entailed three very important investigations. Firstly, it was imperative to understand the phase evolution pattern to develop a better control over the processing parameters. The phase fields and reaction path for the quaternary system needed to be thoroughly scrutinized. Secondly, the temperature range of reactions and thermal stability of the phases needed to be investigated as this behavior of phase evolution could be due to instability of the carbides. Also, the thermal stability of carbides needed to be investigated for better wear resistance during practical applications of the surface engineered components. Thirdly, it was important to investigate the effect of this oscillatory behavior of phase evolution on the mechanical, tribological and oxidation properties of the coating. This is necessary, as if such a variation exists; it is possible to formulate coatings as per application by simply varying the processing power. The following sections (4.3 and 4.4) deal with these aspects of the study respectively.

4.3 Prediction and Verification of Phase-Structure Evolution

4.3.1 Computational Thermodynamic Evaluations

As mentioned in the introduction to the thesis, the current study was aimed at achieving a carbide coating, within an iron based matrix, on the surface of steel via LSE. The carbide coating was achieved by *in-situ* growth of the particles from elemental powders. It was also observed that the X-ray diffraction spectra varied with power used for processing. Hence, there was a need to optimize the parameters used for the process and develop a control over the phase evolution. This is because changes in phase composition and hence

microstructures can have a major impact on the properties. [68] The effect of the variation on properties is discussed in later sections (4.4.1-4.4.3).

It might be useful to look into thermodynamic calculations to estimate the relationship between different phases under the current processing conditions. The primary solidification phases, their phase fields, stability, the reaction path and the possible reasons for their evolution needed thorough investigation to enhance the understanding of the process. Since it would be very cumbersome to experimentally investigate each variable, computational thermodynamic calculations were employed. The use of such techniques makes the design of experiments more practical and efficient. Computational thermodynamic calculations have been employed in the past for microstructural evolution during laser surface alloying process [69]. It was anticipated that with the help of this study, an optimum set of parameters can be estimated.

Phase diagrams graphically represent the equilibrium phases as a function of temperature or composition assuming pressure is kept constant. Awareness of thermodynamic equilibrium is an important factor in understanding properties of different materials and processes. Since the phases evolved during laser treatment vary according to power, (i.e. heat input for a fixed speed), it could be hypothesized that studying the phase diagram of the precursor alloy would give valuable information on the system. It is a known fact that laser surface treatment of materials is more or less a near non-equilibrium process. But, an in-depth analysis of the various phase fields, the stability of phases and effect of compositional variations could act as a guideline which could be extended to such near non-equilibrium conditions under certain assumptions.

The experimental results have been correlated to the computational calculations by considering the stability between the phases deduced from XRD analysis. These phases include BCC (Fe-Cr), FCC (TiC), M_7C_3 and liquid. The coating precursor composition (20 Ti, 20 Cr, 5 C and 55 Fe, all in wt %) was entered in the calculations. The system size was chosen as 1 mole and the calculations were done at 1 atm pressure. The phase diagram resulting from the calculations is presented in Fig 10. The figure also includes a higher resolution image of portion of the phase diagram at higher temperature (1551-1554 K) and C content (4.75-5.00 wt% C).The various phase fields are marked in the diagram. For most of the composition and range, the BCC and FCC phases are stable. The maximum amount of C the coating can have 5 wt%. The M_7C_3 (M= Fe, Cr) is stable only for higher C percentages (>4.5 wt %). According to the phase diagram, at temperatures higher than 1700 K, the only stable phases are liquid and TiC. During laser processing, a melt pool was generated due to interaction of the laser beam and precursor deposited substrate. These calculations were extended to the solidification of the melt pool. Hence a path for the reactions taking place in the melt pool can be traced. The various temperatures at which calculations were done indicated that liquid phase (can be assumed to have a uniform composition) exists for temperatures greater than 2550 K. The Scheil module [57,58] of the software was used to calculate the sequence of phase evolution from the liquid phase. This module is based on the Scheil Gulliver model which assumes fast diffusion in the liquid and no diffusion in the solid phase. These assumptions can be extended to laser processing conditions, as during solidification of the melt pool, rapid rate of the process does not allow any diffusion in the solid phase during processing. Calculation was started from a temperature of 2600 K (approx 50 deg higher than the

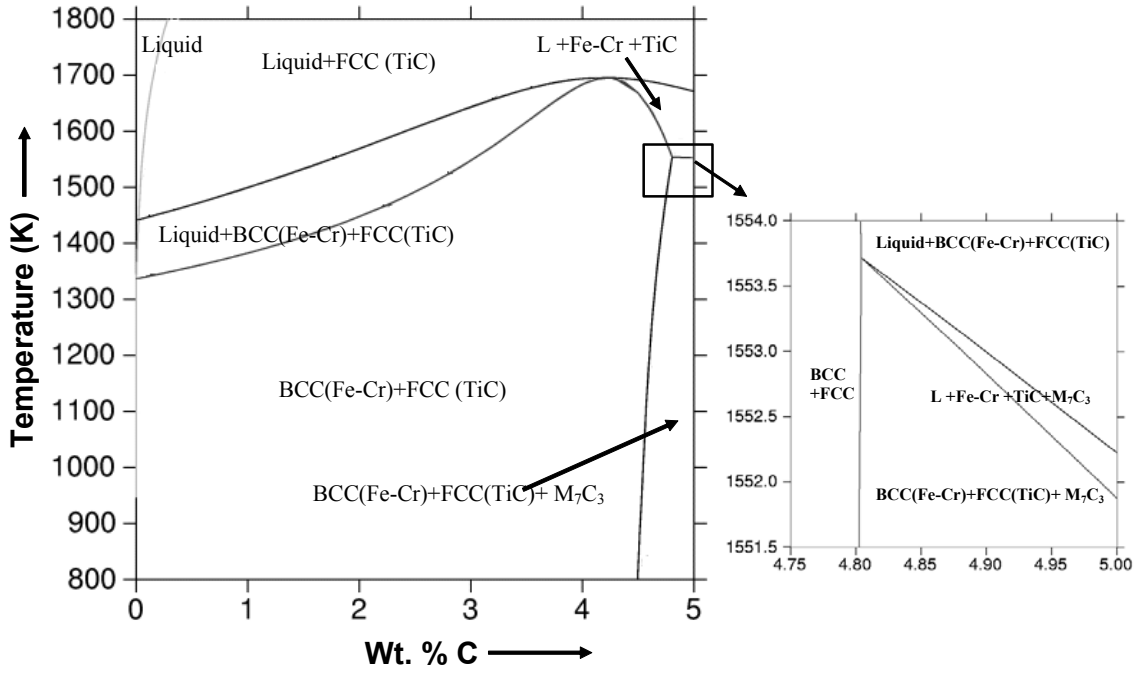

Figure 10: Calculated phase diagram for the quaternary alloy coating.

temperature at which only liquid phase exists) and it was lowered in 1 K steps. The calculation was repeated till no liquid was left.

The results of the analysis are shown in Fig 11. The first phase to precipitate from the liquid is the FCC phase (TiC). Further cooling indicated the sequence of phase appearance was Fe-Cr (BCC) followed by M_7C_3 (complex hexagonal carbide). The calculated terminal solidification temperature was 1560 K (1287 ^oC) at which the mole fraction of the solid phases is equal to 1. Hence the solidification path can be summarized as

Liq. ⟶ Liq. +FCC ⟶ Liq. + FCC + BCC ⟶ Liq. + FCC + BCC + M_7C_3

(PQ ⟶ QR ⟶ RS ⟶ ST)

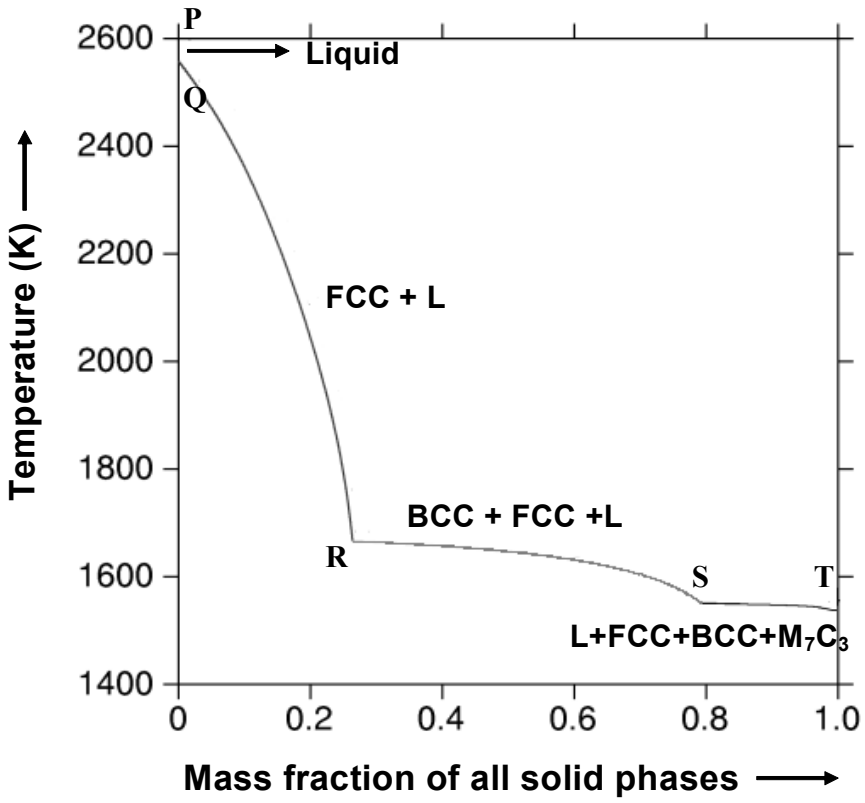

Figure 11: Solidification path traced using calculations based on Scheil assumptions.

It can be interpreted from the results of calculations based on Scheil Gulliver model that M_7C_3 is the last phase to solidify and could be absent while solidification under certain processing conditions. This could be one possible reason for the phase evolution behavior.

Thorough analysis of the current process suggested that the prime variables involved in the process are laser power, scan speed and the composition. The scan speed was kept constant. The laser power was varied over a range (900-2100 W) and effects due to variation in laser power have been observed. Variation in laser power varies the heat input which in turn is expected to affect the type and nature of reactions among compositional species (coating and substrate elements). It is therefore appropriate to understand the effects of the coating elements on the phases evolved. This compositional investigation cannot be done experimentally for a huge set of variables. Hence the phase diagram of the quaternary alloy and other calculations were performed using computational techniques. The phase which was oscillating according to the XRD spectra is M_7C_3. Here M stands for Fe and Cr which suggested that the ratio of Fe/Cr had an impact on the presence of this phase. The phase diagram was plotted as temperature versus the weight % of iron (Fig 12a). The effect of wt% Fe on the amount of phases formed is plotted in Fig 12b. The plot was generated at 1400 K. This temperature was chosen on the basis of calculations based on Scheil module (Fig.11). The calculations indicated that the last solid appears at a temperature slightly higher than 1500 K. Hence, a temperature of 1400 K was chosen for all computational calculations, as it could be safely assumed that the solidification is complete by this temperature (accommodating the undercooling due to the high cooling rate associated with laser processing). It was

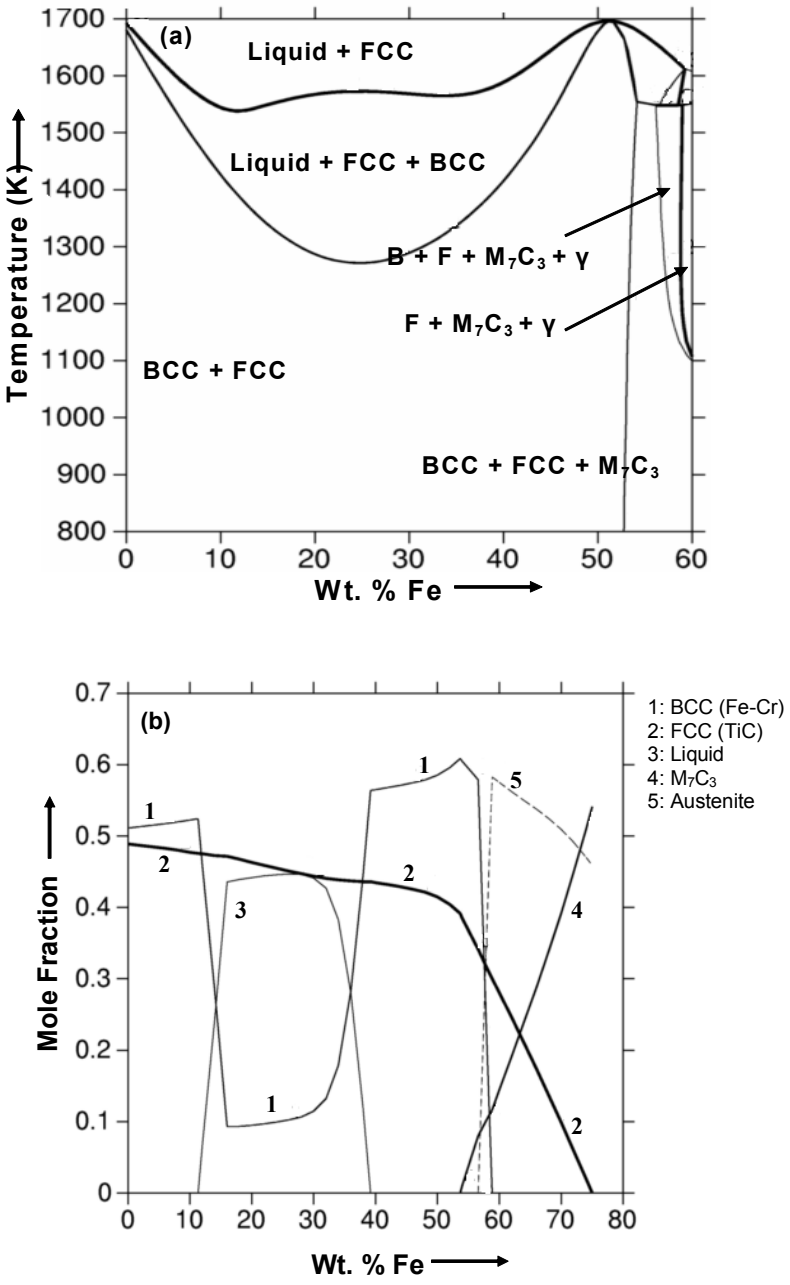

Figure 12:(a) The multicomponent (Fe-Ti-Cr-C) system phase diagram. (b) Mole fraction of all phases calculated at 1400 K for the current alloy composition.

observed that the main phase field still is Fe-Cr and the TiC. But the key point to note here is that below almost approximately 52 wt. %, the M_7C_3 phase is absent.

At Fe compositions higher than this, the M_7C_3 phase is seen to be stable till approximately 1550 K. Quantitatively; the mole fraction of this phase is zero for Fe content lower than 52 wt. % (Fig. 12b). For low Fe percentages, (10-40 wt %) the liquid phase exists at this temperature. The amount of TiC in the composite layer remains constant till this composition and then gradually starts to decrease as mole fraction of M_7C_3 increases. The Fe-Cr phase reaches a maximum around this composition and beyond this Fe and Cr tend to precipitate as M_7C_3 carbides. Since a high amount of C has been included in the precursor alloy, for higher percentages of Fe, the FCC form of iron (austenite) tends to be stable as shown by the dotted line in the figure. Hence, the oscillatory behavior of phase appearance might be observed due to localized compositional variation during laser processing. This is possible as the current composition (55 wt.% Fe) is very close to the M_7C_3 phase boundary. Another potential reason could be that with the current composition, the amount of M_7C_3 could be very low (for samples processed at 1300 and 1900 W) to be detected during XRD. Thus, the parameters which could possibly influence the amount of carbide formed during processing were investigated in terms of wt% C in the coating and Fe/Cr and Fe/Ti ratios. Calculations for amount of M_7C_3 and TiC for 3 different Fe/Cr ratios, 1.5, 2.75 (current precursor composition) and 4 were done. Similar calculations for Fe/Ti ratio were done. These ratios were obtained by varying the wt. % Fe and Ti or Cr by 5wt. % in order to investigate the effect of the relative amount of the elements (Tables 8). The system size considered for calculation was equal to 1 mole and the temperature used for calculations

Table 8: Variation of amount of phase with (a) Fe/Cr and (b) Fe/Ti ratios.

(a)

Fe/Cr (wt% ratio)	M_7C_3 (moles)	TiC(moles)
1.5	0.046	0.3625
2.75	0.036	0.3683
4	0.13	0.37

(b)

Fe/Ti (wt% ratio)	M_7C_3 (moles)	TiC(moles)
2.75	0.036	0.3683
4	0.144	0.28
6.25	0.26	0.192

again was 1400 K. These values indicated that both the Fe/Cr and Fe/Ti ratios have a strong effect on the amount of carbides formed. A Fe/Cr and Fe/Ti ratio of 4 was found to have appreciable amount of the M_7C_3 carbide. Furthermore, since the amount of C in the coating could have a strong bearing on the amount of carbides formed, the amount of phase formed as a function of wt% C was investigated. The results of these calculations are presented in Fig. 13. These calculations were also done at 1400 K for 1 mole system. At this temperature, the liquid phase is stable for a very low C wt. % in the coating (< 2wt. %). The austenite phase exists for higher C contents (> 5wt %). Ti is a strong carbide former and hence TiC was present even for a very low amount of C.

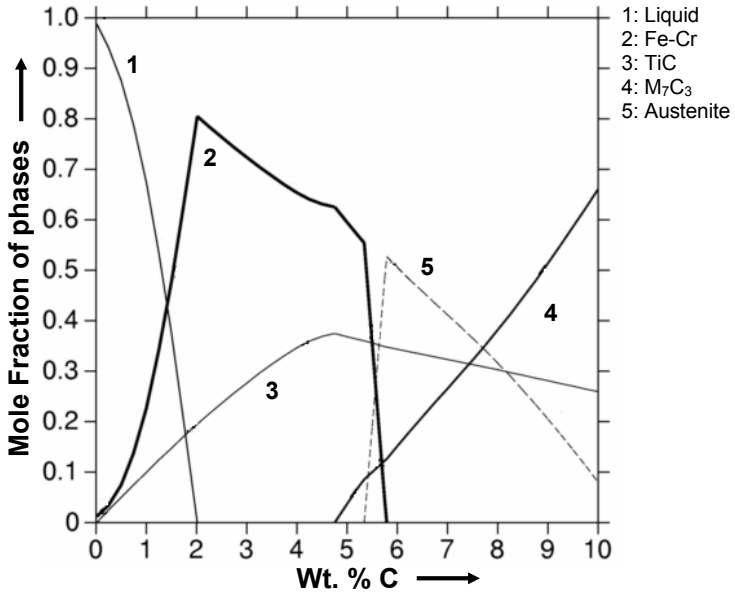

Figure 13: Mole fraction of phases with increasing amount of C in the precursor powder mixture.

Appreciable amounts of the bcc phase (Fe-Cr) is present up to 2.5 wt% C, thereafter it decreases gradually as chromium gets engaged in the formation of carbide. The key thing to note is that for a higher C percentage (7.3 wt. %), equal amount (mole fraction 0.275) of both the carbides could be achieved. This suggests that with a variation in the precursor composition, equivalent amount of carbides can be formed and hence a mixed carbide coating can be achieved.

With the dual aim of investigating the stability of phases with temperature and quantify the maximum amount of this carbide formed for the current amount of C (5wt.%) and Fe/Cr (2.75) and Fe/Ti (2.75) ratios, calculations were done for the mole fraction of the phases against temperature (Fig. 14).

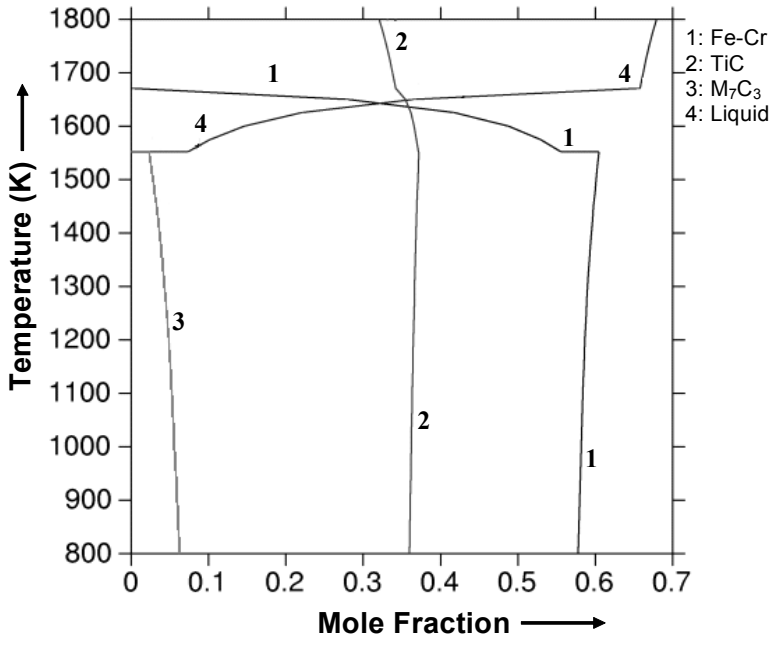

Figure 14: Calculation of thermal stability of the phases.

The calculations were done in the range of 800 to 1800 K with the total number of moles equal to 1. The maximum amount of M_7C_3 which exists in the coating is 0.06 moles. This carbide tends to disappear at 1553 K. The Fe-Cr (solid substitution alloy) phase is stable till 1670 K and disappears at higher temperatures. TiC is found to be stable till very high temperatures (T>1800 K) which indicates that the carbide is thermally stable till very high temperatures. The stability of the carbides is further being tested and verified using experimental techniques (DSC) as the thermal stability of the phases is imperative for enhanced wear properties of the coated sample. Although the computational calculations discussed in this section are difficult to readily and exactly extend to laser processing conditions (non equilibrium in nature), they relatively closely confirm and provide relationships between compositional elements and temperature for evolution of various phases. Such information is vital in providing the guidelines in selection and design of experimental parameters for tailoring coating properties. Further experiments would be based on the conclusions drawn as part of this computational effort.

4.3.2 Analytical Evaluation: Differential Scanning Calorimetry

Evolution of the primary solidified phases and their phase fields was computationally evaluated for equilibrium (Fig. 10) and near non-equilibrium (Fig. 11) conditions and discussed in the previous section. Phase evolution and their stability play an important role in the functional properties of the coating and hence it was necessary to experimentally verify the temperature range of phase evolution and the thermal stability of the phases in the coating. Since, a variation in evolved phases with laser processing power (heat input) at a constant scan speed was observed during X-Ray Diffraction

(XRD) analysis and this could have an effect on hardness, wear, and oxidation properties, process optimization to tailor the properties according to application was crucial. The thermal transitions and temperature range for reactions (computationally evaluated earlier) needed to be experimentally verified. Differential Scanning Calorimetry (DSC) has been a long established process for thermal investigations [70,71,72]. Although the heating/cooling rates attained during LSE can be far different than that are available for DSC runs, the perception behind the current effort was as follows. XRD analysis (for laser processed samples) and computational evaluation for Scheil Gulliver assumptions (no diffusion in solid) [57,58] indicated formation of equilibrium phases. It is therefore considered reasonable to conduct DSC studies for identification and verification of phase transition events in the precursor powder mixture and correlate them with the events occurred during LSE. The vision behind investigations using DSC is that an insight into the temperature range of various carbide forming reactions can be achieved. In addition to that, the temperature ranges of other thermal events during heating and cooling of the precursor powder mixture can be captured. With any change in the heat capacity of the specimen, heat of transformation for the reactions could be investigated. It is envisioned that this set of information coupled to the computational evaluation (presented earlier) would help in developing a thorough understanding of the nature of phase transition in the precursor powder mixture (with composition same as used for laser processing) and help in tailoring properties according to the desired application.

The events observed during DSC runs have been presented in Fig. 15. Some small fluctuations were seen in the heating curve at lower temperatures (450-600^{o}C), (marked

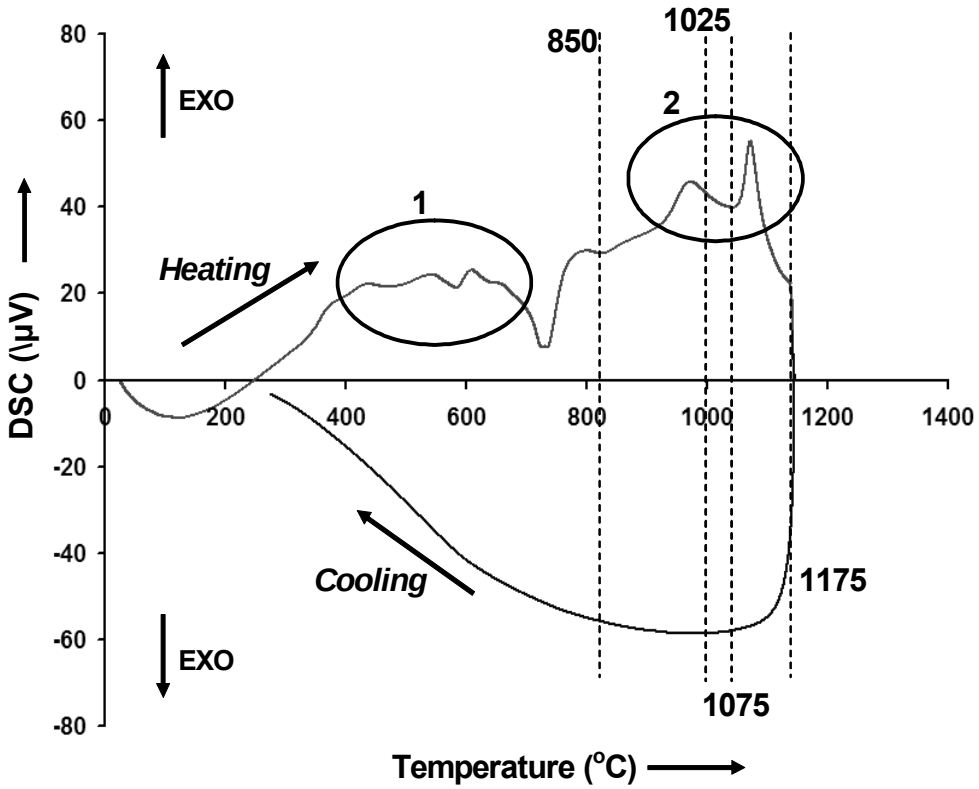

Figure 15: DSC curves for heating and cooling of the precursor powder mixture at the rate of 40°C/min in Argon atmosphere.

as ellipse 1). These fluctuations could either be due to particle rearrangement or surface degassing. These fluctuations occur at very low temperatures and are not major events. Hence it could be assumed that these do not affect the process. An endothermic event was observed in the temperature range of 650-800 ^{o}C. This event could possibly be a (α-Fe) → (γ-Fe) transition. DSC runs for pure Fe were done and such endothermic event occurred during that although at a higher temperature. This suggested that the endothermic event could be the ferrite to austenite transition of Fe. The range of temperatures on which this transformation was observed was much lower than the conventional transition temperature. This could be attributed to the presence of other elements (20 wt% Ti, 20 wt% Cr and 5 wt% C) within the powder mixture. The best possible way to confirm this hypothesis would be to conduct a high temperature *in-situ* XRD for the powdered sample. At higher temperatures (890- 1150 ^{o}C), twin exothermic events were observed (marked as ellipse 2 in Fig.15). The presence of these exothermic peaks could be attributed to the carbide forming reactions. There were no events observed while cooling. This indicated that all the powders had reacted by 1175 ^{o}C.

Results for re-run (second run for same conditions) have been presented in Fig.16. Neither the heating nor the cooling cycle indicated any events till 1175 ^{o}C. The minor fluctuations, endothermic and exothermic events were absent for the powder mixture during this run with an indication of irreversible transformation of phases evolved in the first run. The temperature ranges in which the events took place during the first run have been marked on the figure. Although the DSC plot gave the temperature range of thermal transitions, they are not very informative unless interpreted. Some

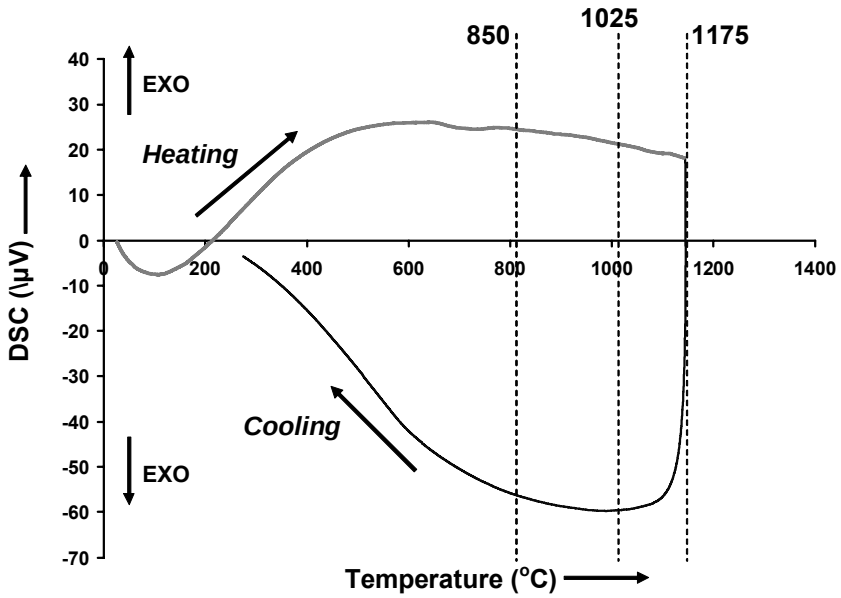

Figure 16: DSC heating and cooling curves for re- run of Fe, Ti, Cr and C powder mixture.

analysis of the plots is required to understand what the transitions possibly could be. The temperatures (850, 1025, 1075 and 1175 ^{o}C) have been marked on Figs. 15 and 16 to indicate four temperatures at which analyses, to identify the occurring thermal transitions, were done.

The DSC plots can be interpreted either by varying the sample parameters (like mass, composition) or by variation of operating parameters (rate of heating and atmosphere used). [73] The heating rate and the atmosphere used were kept constant in the current case. The composition of the powder mixture was varied to interpret the events and to investigate the effect of Fe in the mixture. DSC runs on a powder mixture of Ti, Cr and C (4:4:1 in wt%) was conducted and the plot is shown in Fig. 17. The DSC runs were again done at 40^{o}C/min in Argon atmosphere. Exothermic events similar to the ones

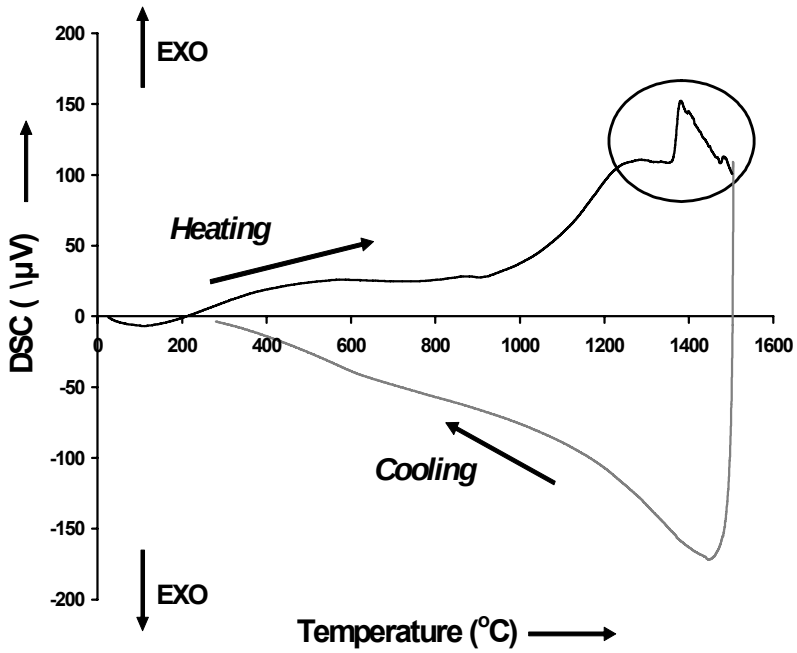

Figure 17: DSC heating and cooling curves for Ti, Cr and C powder mixture at 40°C/min in Argon atmosphere.

present for the precursor powder mixture (Fig. 15) were observed. However, no endothermic transition was observed. This proved that the endothermic event in the precursor powder mixture (Fig. 15) was due to the presence of Fe and is (α-Fe) → (γ-Fe) transition. Another noteworthy point to be observed was the temperature at which the exothermic reaction took place (1350-1500 °C in Fig.17). This was much higher than the temperature range of reactions (890-1150 °C in Fig. 15) for the precursor powder mixture (Fe, Ti, Cr and C). Hence, it could be interpreted from the DSC curves that the presence of Fe in the precursor mixture lowered the temperature for the exothermic events (possibly carbide forming reactions).

Coupling of results obtained by DSC with other structure sensitive analytical techniques (like X-ray diffraction) would help in thorough understanding of the occurring

events. [73] Since no event was observed during cooling, the thought behind the XRD runs was that the evolved phases should be present at room temperature i.e. the arrested phases could be identified using this technique. X-ray diffraction analysis of the DSC run samples had strong background signals which made analysis susceptible to errors. The strong background signals could be attributed to the presence of backing material on which the small amount of powder mixture (~78 mg) was mounted. With the aid of an appreciable amount of powder (obtained by heating the mixture of powder in Infrared furnace) and a very slow X-ray scan, the background signal was minimized. The samples were heated in the furnace at temperatures corresponding to events in DSC plots (marked in Fig. 15). The XRD spectra for all conditions have been presented together in Fig.18 (a-d). The XRD spectra revealed that no reactions took place till 850 ^{o}C (Fig. 18a) and the peaks (as marked) are un-reacted powders in elemental state. The sample heated to 1025 ^{o}C (Fig 18b) indicated that carbide forming reactions had started to take place, but sufficient amount of carbides had not formed till this temperature. This confirmed another fact that the Infrared furnace heated samples (heated under identical conditions) followed the events of DSC plots. Fe and Cr both have a bcc crystal structure and have near equal atomic radii also (2.48 and 2.49 Å) and their characteristic peaks almost overlap each other. The powder mixture heated to 1075 ^{o}C revealed the presence of various carbides and the spectrum (Fig. 18c) indicated that the majority of the reactions had started to take place. The major phases present were TiC, Fe-Cr, M_7C_3 (M = Fe and Cr), Fe_3C and some graphite. The powder mixture heated to 1175 ^{o}C (Fig. 18d) indicated the presence of similar phases (as that for 1075 ^{o}C). As the DSC plots revealed, all the exothermic events had taken place and the reactions were completed by this temperature.

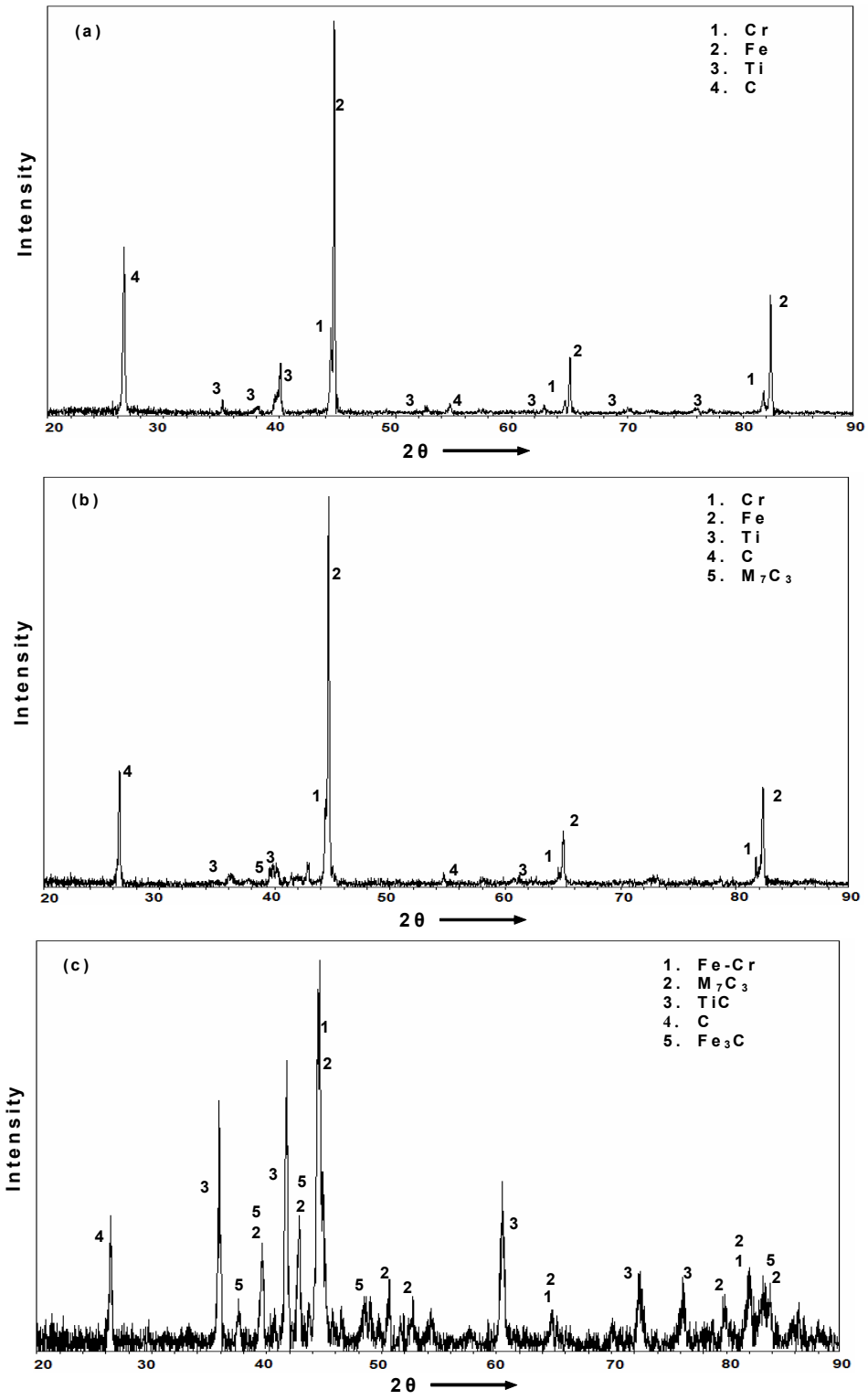

Figure 18: XRD spectra for furnace heated samples. (a) 850 ^{o}C, (b) 1025 ^{o}C, (c) 1075 ^{o}C, (d) 1175 ^{o}C.

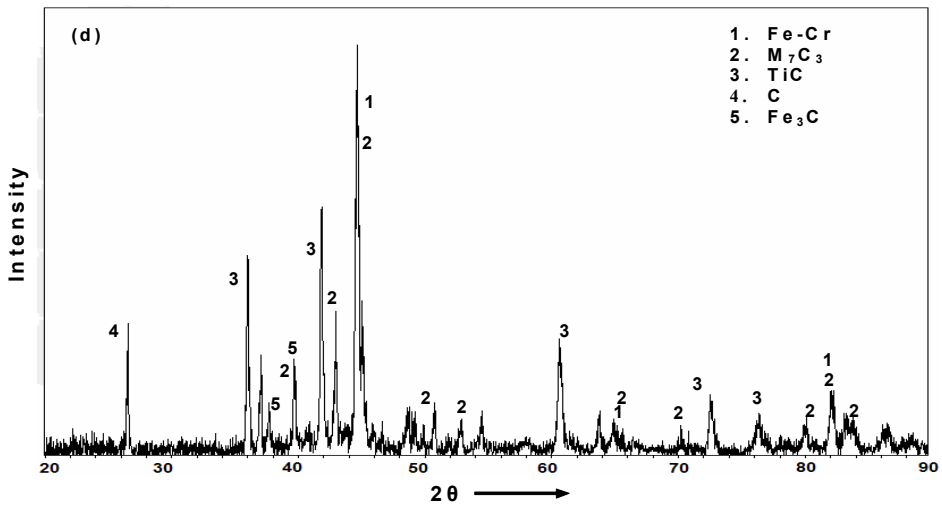

Figure 18: Continued

The powder mixture had reacted and hence no events were seen on cooling the reacted mixture. The phases formed during heating of the powder mixture in the furnace were also found in agreement with the phases predicted by computational calculations. The computational calculations based on Scheil Gulliver solidification model, indicated that the terminal solidification temperature was 1560 K (1287 ^{o}C). This was the reason that all computational calculations were done at 1400 K (1127 ^{o}C) to accommodate the effect of undercooling due to the high cooling rate associated with laser processing. The choice of temperature was corroborated by DSC experiments which indicated that almost all the reactions take place in the range of 1000-1175 ^{o}C. Hence, the computational results are in accord with the experimentally evaluated results.

Some key interpretations could be made from the results obtained from the coupling of DSC and XRD results. From the observations of the re-run of the mixture of Fe, Ti, Cr and C (Fig. 16) and the XRD pattern (Fig. 18a) for the sample heated till 850

^{o}C, it can be concluded that the endothermic fluctuations in the DSC plot at lower temperatures (450-600^{o}C) did not represent any reactions and was probably particle rearrangement or surface degassing. It can be inferred from Fig.15 and Fig.17 that the other endothermic (650-800 ^{o}C) event was due to the elemental iron in the powder mixture. Since there was no other reaction (event) observed till this temperature, it could be assumed that the powders had not reacted until this temperature. Once the powders reacted, to form certain phases after the completion of the heating cycle, a reverse transition was not observed during the cooling cycle (Fig.15) or during the re-run (Fig. 16). This substantiates the fact that majority reactions had taken place and no elemental un-reacted powder was left. The twin exothermic events observed at higher temperatures (>850^{o}C) represented carbide forming events (Fig. 15 and Fig. 18). Similarly, the exothermic peaks observed in Fig.17 were identified to be events associated with formation of Ti and Cr carbides. The XRD spectrum that confirmed the presence of Ti- and Cr- carbides has not been provided here as this route was adopted just for qualitative understanding of the peaks. The amount of energy released as a result of the reaction could be gauged from the general equation for the formation of titanium carbide, Ti + C $\rightarrow$ TiC (ΔG = -186606 + 13.22T J/mol). [41] The formation of the carbides could be attributed to the strong carbide forming tendency of the elements. The Fe and Cr powders form a solid solution Fe-Cr (bcc) with the lattice parameter of 2.88 Å and hence the Cr diffraction peaks (Fig. 18a, b) were no longer visible in the XRD spectra at higher temperatures (Fig 18c,d). The key fact to note from the XRD results was that all the other phases, with the exception of Fe_3C and graphite, had also been seen in the XRD spectra for laser processed samples [68] with the coating formed using the same precursor powder

mixture. This corroborates the fact that although the heating and cooling conditions during LSE are different from that used here, it is reasonable to conduct DSC studies to develop a thorough understanding of the phase transition events and correlate it with events during laser processing.

Iron was used as the major element in the precursor for the coatings on 1010 steel to avoid any difficulty with chemical compatibility. The carbides have good compatibility and wetting characteristic with Fe [40]. Also, since the substrate is 1010 steel, good bonding was expected. In addition to that, the other advantage of using Fe in the coating precursor powder mixture deduced from this study was that its presence lowers the temperature of the exothermic events by almost 300 ^{o}C (Fig. 15 and Fig. 17).

One of the main aims of the study was to understand the temperature range of reactions. The XRD spectra (Fig 18 a-d) suggested that no reaction took place till 850^{o}C; some reactions had begun by 1025 ^{o}C while reaction completion takes place between 1050-1175 ^{o}C. But from the DSC plots obtained during experiments, it was difficult to interpret the exact temperature of the reactions due to partial overlap of the exothermic peaks. Also, since the plot could not be used directly for evaluating thermodynamic potential function (heat of reaction), de-smearing of the overlapping peaks needed to be done. The advanced peak separation software (NETZSCH peak separation) was used to evaluate the data. By using interpretations from DSC results and XRD analysis, it was possible to represent the DSC plot as a superposition of peaks. The baseline was made horizontal by subtracting the DSC profile from the plot for re-run sample (subtracting Fig. 16 from Fig. 15). The FRASER-SUZUKI profile was used for separation of peaks. This profile is the best for thermo-analytical measurements. It basically represents a

asymmetric gauss profile i.e. for asymmetry equal to zero, it corresponds to a Gaussian profile. [74] The equations used for the calculation of signal and area under the peaks (for Fraser Suzuki profile) are given by [74]

$$y_{Fraser} = Ampl.\exp[-\ln 2[\ln\{(1+2.Asym.(x-Pos)/Hwd) \div Asym\}]^2]$$

$$A_{Fraser} = 0.5.\sqrt{\prod / \ln 2}.Ampl.Hwd.\exp[Asym^2 / 4\ln 2]$$

where y_{Fraser} represents the signal and A_{Fraser} represents area under the separated peaks. *Ampl* is the amplitude of the peaks (difference between the baseline and curve), *Hwd* is half width of the peaks, *Asym* is asymmetry and Pos the peak position.

An evaluation range of 850-1150 ^{o}C was chosen on the basis of XRD analysis and the events during DSC runs as no reactions took place at temperatures lower than this. Within the evaluation range, the approximate peak positions for the twin exotherms were marked. The amplitude, half width and asymmetry were initialized. Visual optimization of the separated peaks was done by varying the parameters (*Asym, Pos, Hwd and Ampl*) to manually achieve a reasonable curve fit. Finally, a non linear regression was employed to achieve the best possible fit. The coefficient of correlation achieved was of the order of 0.9937. The results of calculation have been presented in Fig. 19. Sep-1 and Sep-2 represent the first and second separated peaks. The section of original DSC plot has also been shown in the figure. The time and temperature scale were plotted on the X-axis while the calibrated DSC signal (heat flow, mW/mg) was chosen as the Y-axis. The details of area under the peaks, onset and endset temperatures have been presented in Table 9. The peak positions were found to be 1003 and 1073^{o}C. The onset and endset temperatures of peaks were 889 and 1049 ^{o}C; and 1129 and 1104 ^{o}C respectively. This

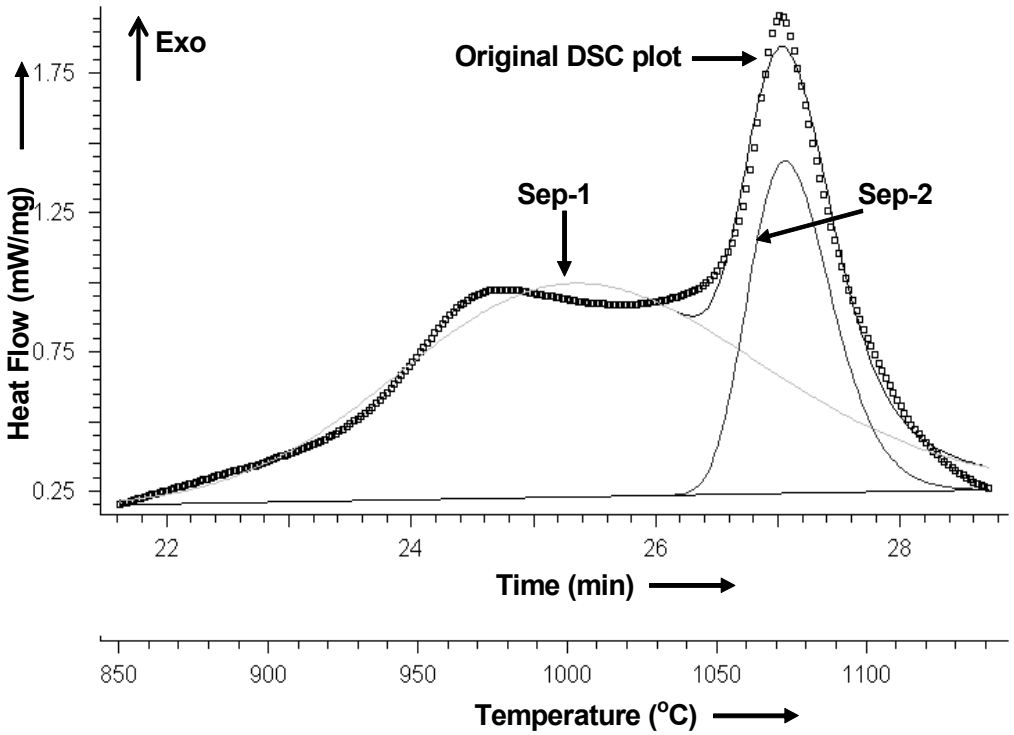

Figure 19: Fitting with 2 peaks of Fraser-Suzuki (asymmetric gauss) profile for DSC twin exothermic event.

Table 9: Evaluation of separated peaks obtained by de-smearing of twin exothermic DSC events.

Peak	Position (°C)	Area (J/g)	Onset (°C)	Endset (°C)
SEP-1	1003.48	169.30	889.82	1129.77
SEP-2	1073.77	60.56	1049.93	1104.521

suggested that the event associated with the first peak (SEP-1), took place over a longer range of temperature.

The temperature values match well with the results obtained by XRD analysis. The XRD analysis suggested that no reactions were observed till 850 ^{o}C. Also, no TiC formation was observed till 1025 ^{o}C although some M_7C_3 was found to occur at this temperature. The next set of experimental results, XRD spectra for 1075 and 1175 ^{o}C, suggested the formation of both TiC and M_7C_3 (Fig. 18c,d). Thus it could be interpreted that the wide peak Sep-1 represented the initiation of formation of the M_7C_3 phase while the narrow peak (SEP-2) represented the initiation of formation of TiC. The exact range of M_7C_3 cannot be marked as there are other evolved phases also (Fe_3C and Fe-Cr). But, it could be interpreted that for the current system, TiC forms in the temperature range of 1050-1104^{o}C. In any case, it was deduced that the range of exothermic reaction was within 889 - 1130^{o}C.

The rerun of the samples (Fig. 16) was done to investigate the stability of the reaction products. The thermal stability of the carbides was a vital issue for coatings dedicated for wear resistant applications. This made the thermal stability investigations via the re-run imperative. Since no event was observed during the re-run for the given system, it could be concluded that the evolved phases were thermally stable till this temperature. Also, since the carbide particles grew *in-situ*, better bonding with the matrix was achieved. Such a thermally stable carbide coating with particles well bonded to the matrix and uniformly distributed will have superior wear resistance. The wear and oxidation results for the laser processed coating have been presented in the following sections. In addition to DSC runs on the precursor powder mixture, thermal stability of

the coating was investigated by DSC experiments on a section (slice) of the laser-processed coating. The DSC plot for this run is shown in Fig. 20. Thermal stability was investigated till 1525 ^{o}C (1798 K). When two surfaces rub against each other (as in case of wear applications), the temperature at the point of contact rises. Hence, stability of phases is desired. No thermal event was observed during the heating and cooling cycles and all the phases were found to be stable until the temperature. The computational evaluations done earlier indicated that majority of the phases are stable till 1550-1600 K. Experimental results for the laser-processed sample indicate much higher thermal stability (1750-1800 K).The difference in temperatures could be

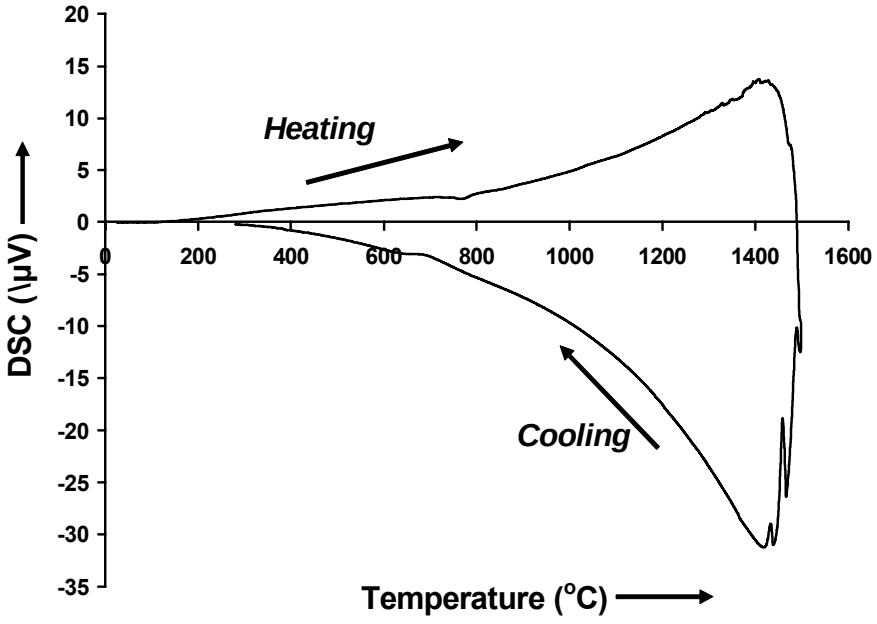

Figure 20: DSC runs for laser processed coating (processed at 1.5 kW) at 40^{o}C/min in argon atmosphere.

attributed to the different conditions under which the coating was processed in comparison to the equilibrium nature of computational evaluation.

The information obtained from the present study is thus extremely important for two reasons. Firstly, it can be used to tailor the process in terms of processing power and laser scan velocity to regulate the heat input and thus achieve required thermal fields to produce respective phases. Secondly, the coating synthesized for wear applications was found stable till extremely high temperatures. The temperatures achieved due to heat build up during sliding are much lower than these temperatures and hence it can be hypothesized that degradation in wear properties could be delayed.

4.4 Processing Effects on Functional Properties.

4.4.1 Hardness

To correlate the effect of type and variation in the phase evolution with the properties, mechanical characterization was conducted for microhardness, wear, and oxidation properties. In general, microhardness values indicate a tremendous improvement in hardness of the steel substrate due to the laser surface modification. Nearly a 5-fold improvement in the hardness of the surface of the as-received sample processed at different laser powers is observed (Fig. 21). The hardness profile of all the samples indicates that the hardness is higher in the coating region and gradually decreases through the heat affected zone (transition zone) into the substrate. The hardness values show some variation through heat-affected zone. The higher hardness of the coating can be attributed to the *in-situ* formation of various carbides in the coating region. The Knoop hardness

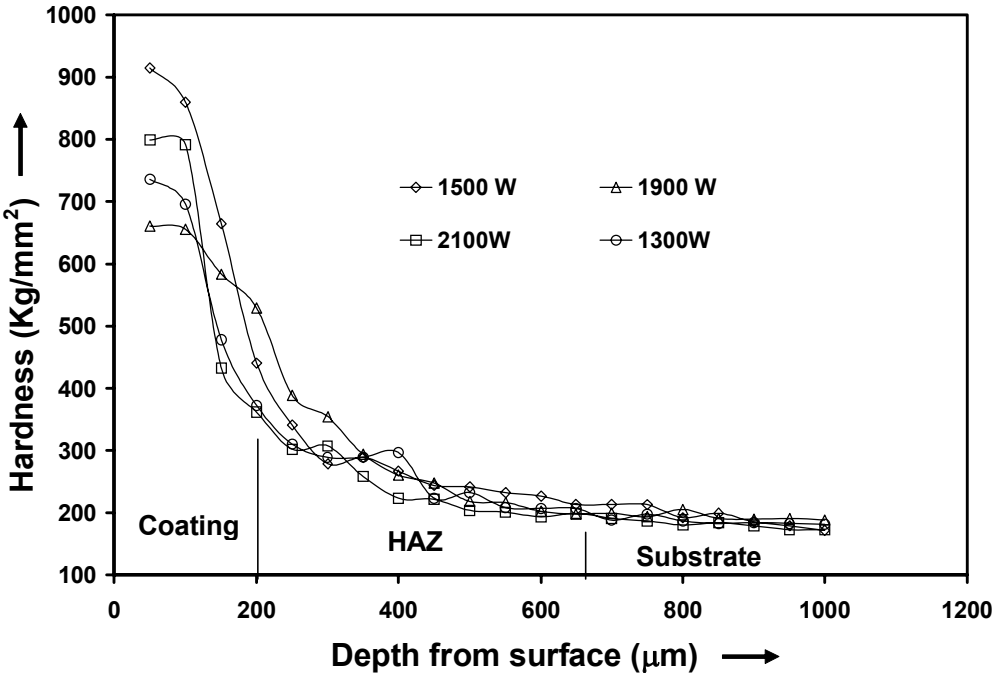

Figure 21: Hardness profiles for laser processed samples.

values in the coating for samples in group 1 (A1 and A2) are higher than the samples in group 2 (B1 and B2) (Fig. 21). The potential reason for this behavior is the absence of Cr- carbides in Group 2 and its presence in Group 1, with TiC being present in both (Figs. 7 and 9). Hence, it becomes imperative to study the phase evolution behavior as the hardness of the coating seems to be a function of the evolved phases.

4.4.2 Wear Performance

The weight loss during sliding wear of the samples is an indicative of the wear resistance of the samples. Hence, lower the weight loss, better the wear properties possessed by the coating. During the dry sliding wear studies, the cumulative weight loss of the laser-processed samples was found to be negligible in comparison to the AISI 1010 steel

substrate (Fig. 22).This clearly indicated a vast improvement in the wear resistance of the steel substrate due to the presence of carbides in the coating region. The weight loss of the coated samples was nearly 4 times less than that for the as-received sample. Also, as the figure shows, the cumulative weight loss of the as-received sample becomes almost constant after some time due to strain hardening effects. Among the samples processed at different powers, it was seen that the sample processed at 1900 W had the worst wear resistance. This is the same sample which has lower hardness and has absence of chromium carbides (Figs. 7 and 9). On the contrary, the other sample from the same group, which had no chromium carbides, B1 (1300 W) indicated very low cumulative weight loss.

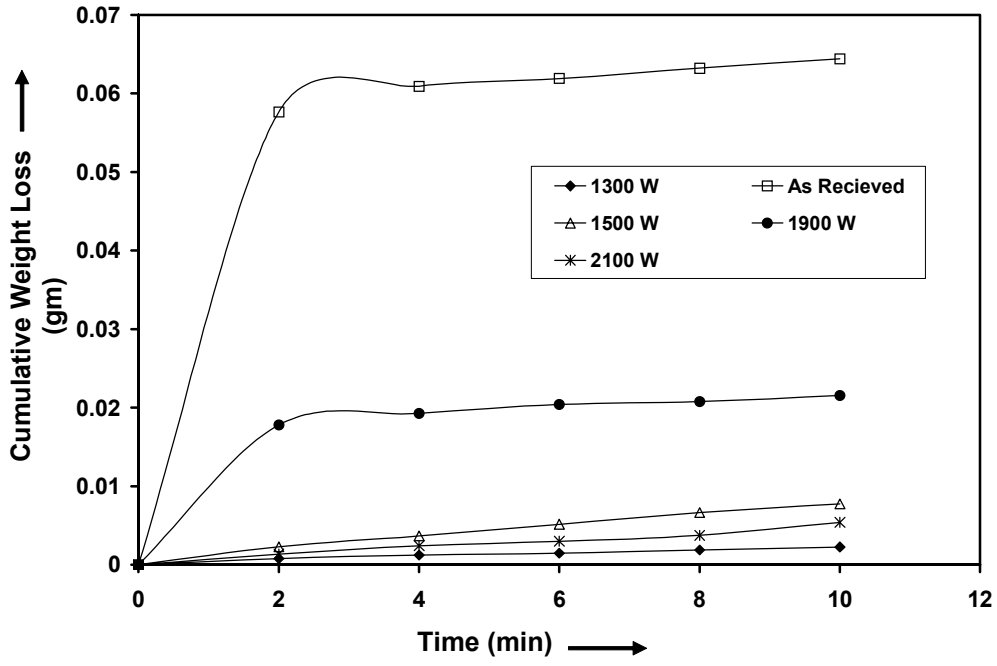

Figure 22: Cumulative weight loss as function of time during dry sliding wear.

Such contrast in wear behavior from the same group of samples could be attributed to the physical nature of the laser processed surface, which was evaluated by surface roughness measurement. The measurements show that for the sample processed at 1300 W (B1), R_a (arithmetic mean roughness) = 9.198 μm, R_z (average maximum height) = 48.2 μm whereas for the sample processed at 1900 W (B2) has R_a =1.476 μm, R_z =9.34 μm. This indicates that the former is relatively rougher in comparison to the latter, thus the surface area of the sample in contact with the wheel during sliding wear was less in the case of B1 and hence the low weight loss.

4.4.3 Oxidation Kinetics

The rate at which metals and alloys oxidize is very important from the engineering standpoint. It was hypothesized, based on DSC results, that the wear resistance of the carbide coating is expected to be good at elevated temperatures due to the stability of the carbides within the laser processed coating. But, the other key issue which needs to be addressed in order to confirm this hypothesis is the oxidation of the coating. The prolonged stay at elevated temperatures (in oxidizing environments such as air) could lead to degradation in the excellent properties of the coating. The oxidation rate is usually evaluated by exposing a specimen in the furnace at a fixed temperature and measuring the weight change as a function of time (known as isothermal oxidation) and is generally expressed as weight gain per unit area.

The oxidation behavior of the composite coating was characterized through measurement of the mass change/surface area (Δm/a) during exposure at 700 ^{o}C and 1000

^{o}C in a TGA. Results for isothermal oxidation (3 hrs. each) of samples processed at laser powers of 1300 W, 1500 W, 1900 W, 2100 W are presented in Fig. 23a and Fig 23b. Here, Δm is the difference of m and m_o, where m= weight at any given time and m_o=original weight in milligrams.

At 700 ^{o}C, the weight gain in the sample processed at 2100 W is the least. It can be seen that the weight gain with time is almost negligible. The sample processed at 1500 W shows the maximum weight gain with time while the samples processed at 1300 and 1900 W appear to oxidize at a faster rate in the early part and gradually stabilize with holding time. The possible reason for such a behavior is that the oxidized film initially forms over the coating and then gradually further reaction becomes a dependent on the diffusion of oxygen through the film. At a higher temperature, 1000 ^{o}C, the oxidation behavior of the composite coatings processed at different powers changes. The least weight gain was still observed in the sample processed at 2100 W. But the maximum weight gain was observed in the samples processed at 1300 and 1900 W, instead of 1500 W (as was the case at 700 ^{o}C). Both these samples appear to gain most of the weight in early part of the hold and the oxidized layer stabilized thereafter. Nearly the same weight gain was observed for both samples (1300 and 1900 W). The rate law governing the oxidation could not be interpreted from the curves directly. These plots indicate that the rate law governing oxidation for most samples is parabolic through out. Such a parabolic rate of oxidation is represented by the following equation, where t is the oxidation time and k and C represent the oxidation constants.

$$(\Delta m/a)^2 = kt + C$$

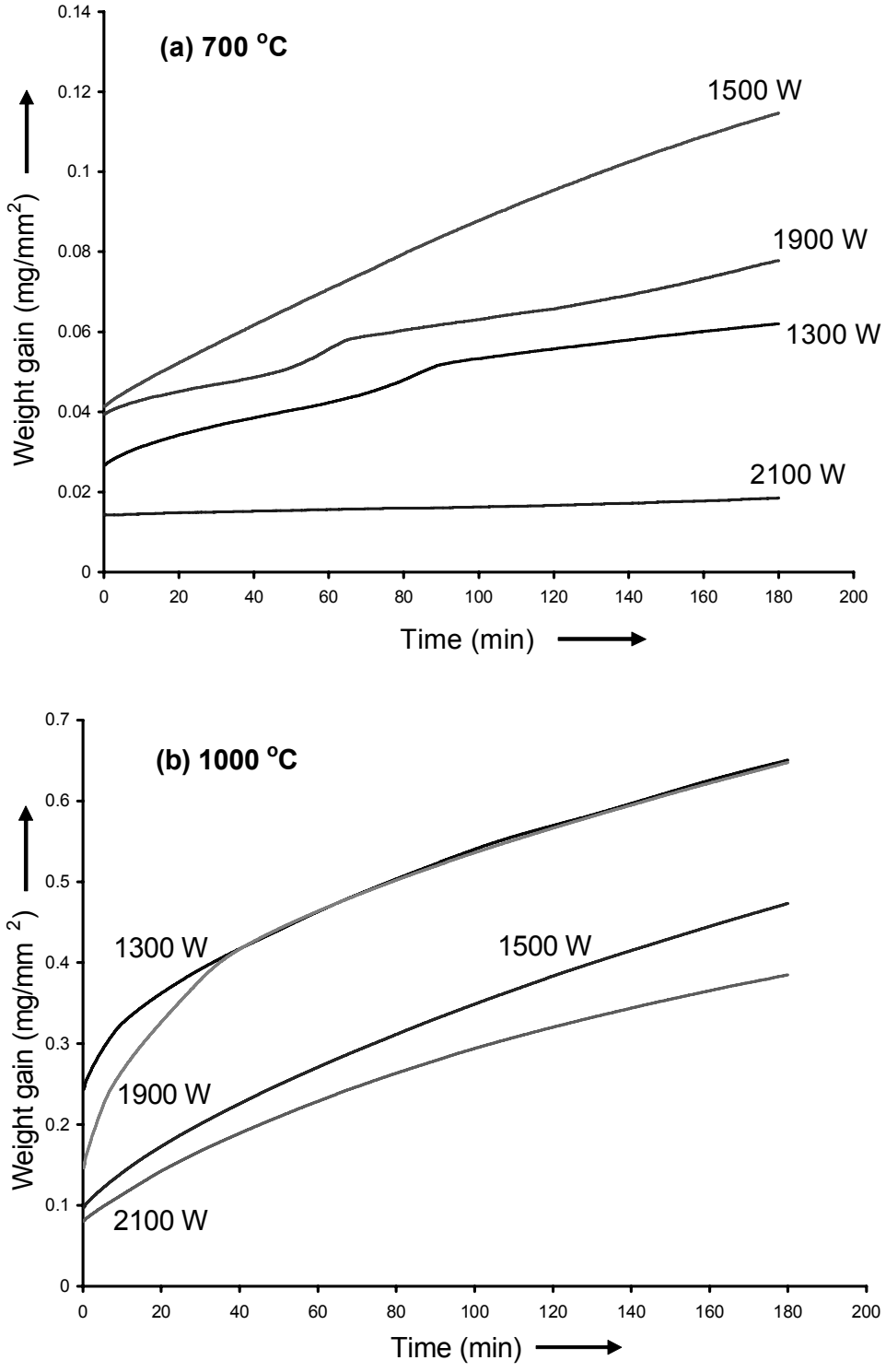

Figure 23: Weight gain as a function of time at (a) 700 °C and (b) 1000 °C.

The plot between $(\Delta m/a)^2$ and time at 700 and 1000 ^oC is presented in Fig 24a and Fig 24b. From the equation, it was interpreted that for the oxidation reactions to be governed by parabolic laws, the lines in Fig 24 would be straight and the slope of the lines would represent the rate constant k. At 700 ^oC, the oxidation rate is parabolic for all the test temperatures during constant temperature exposures with a correlation coefficient better than 0.99 for all the cases. At 1000 ^oC, 1500 and 2100 W samples were parabolic from the start of the isothermal hold. The oxidation took place at a very slow rate and hence the weight gained with time was very low. The samples (laser processed) at 1300 and 1900 W seemed to have oxidized at a higher rate in the early few minutes (~40 min) and thereafter followed a parabolic rate law. The reason for such a behavior was the build up of the initial oxide layer on the surface during the first 40 minutes. The build up of the initial layer is an interface controlled reaction while the subsequent reactions are diffusion controlled as the oxygen has to diffuse through the oxidized layer. Hence, for the samples processed at 1300 and 1900 W, a combination of rate governing laws applies. In comparison, the other 2 samples (1500 and 2100 W) followed the parabolic rate law from the beginning and hence oxidized less. It may be recalled that the former 2 samples (1300 and 1900 W) are the same samples which had one type of carbide present and have similar XRD spectra in comparison to the latter samples (1500 and 2100 W). This could be one of the major factors of the different behavior of the 2 sets of samples. For this hypothesis to be confirmed, longer runs at elevated temperatures followed by XRD analysis needs to be performed to interpret the oxides formed in the 2 cases. The rate constants, k and C, for the isothermal oxidation at 700 and 1000 ^oC are tabulated in tables

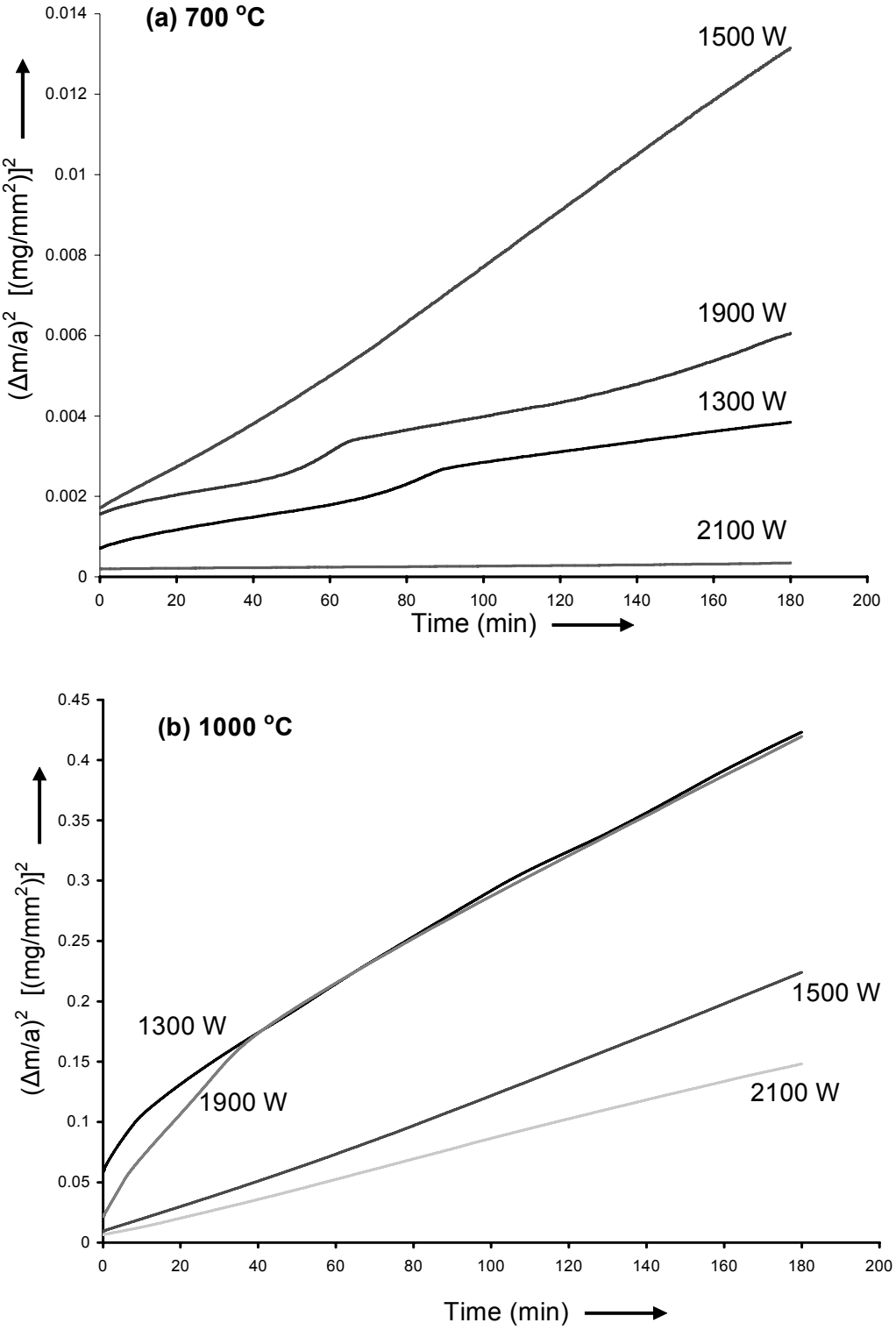

Figure 24: Oxidation kinetics for composite coatings at (a) 700 °C and (b) 1000 °C.

10 and 11. It is visible that for the sample processed at 2100 W, oxidation rate is significantly lower than other test samples. Another key fact to be observed was the overall rate of oxidation in samples without any chromium carbides was nearly equal at both 700 and 1000 ^{o}C. But overall, it was observed that the oxidation kinetics all the carbide composite coatings followed the parabolic rate law which indicated superior oxidation resistance.

Table 10: Oxidation kinetic constants for composite coatings at 700 ^{o}C.

Power (W)	K ($mg^2mm^{-4}\ min^{-1}$)	C ($mg^2mm\text{-}^{4}$)
1300	2.0×10^{-5}	8×10^{-4}
1500	7.0×10^{-5}	1.3×10^{-3}
1900	2.0×10^{-5}	1.6×10^{-3}
2100	7.0×10^{-7}	2.0×10^{-4}

Table 11: Oxidation kinetic constants for composite coatings at 1000 ^{o}C.

Power (W)	K ($mg^2mm^{-4}\ min^{-1}$)	C (mg^2mm^{-4})
1300	1.9×10^{-3}	9.6×10^{-3}
1500	1.2×10^{-3}	3.5×10^{-3}
1900	2.0×10^{-3}	79.6×10^{-3}
2100	0.7×10^{-3}	6.5×10^{-3}

Chapter 5

5. SUMMARY

The current effort was made to conceptualize and optimize the procedure and parameters for laser assisted *in-situ* carbide coating on steel. A systematic step by step procedure was followed to develop a thorough understanding if the laser surface engineering of plain C steel with the quaternary system. The following conclusions can be drawn from the investigations thus far:-

- The information obtained from the present study is thus extremely important for two reasons. It would be used to tailor the process in terms of processing power and laser scan velocity to regulate the heat input and thus produce respective phases.
- The coating was metallurgically bonded and composite in nature. Very fine TiC particles were prominently present in the surface layer of all the samples. The carbide particles were grown *in-situ* (from elemental powders) within the melt pool. Uniform distribution of very fine TiC particles within the coating was achieved and no microstructural inhomogeneity was observed in the coating.
- It was found that chromium carbide was absent in the samples processed at 1300 W and 1900 W. An oscillatory pattern of phase evolution, with respect to power (900- 2100 W), was observed for this phase (M_7C_3).

- A substitutional solid solution of chromium in iron (Fe-Cr) was found in all the samples and the relative estimated amount of the phase was higher for the samples without chromium carbides.
- Metastable phase (characteristic of non-equilibrium synthesis) like martensite was present in the coating and transition zone which contributed in improving the hardness and wear resistance of the coating.
- Computationally plotted equilibrium phase diagram for the quaternary system indicated that for the current precursor composition, Fe-Cr, TiC and M_7C_3 (M = Fe, Cr) were the stable phases till 1553 deg K. The solidification path from a liquid of uniform composition based on Scheil Gulliver model indicated that the first phase to precipitate out of the melt pool is TiC followed by Fe-Cr and finally M_7C_3 carbides.
- For any M_7C_3 carbide to exist, at least 52 wt% Fe should be there in the precursor powder mixture for the current composition. The Fe/Cr and Fe/Ti ratio of 4 was found to have appreciable amount of the M_7C_3 carbide. The amount of phase present varies drastically with wt% C in the coating. For 7.3 wt% C equal amount of both TiC and M_7C_3 carbide could be achieved.
- The thermal stability of evolved phases quantified with respect to temperature suggested that an appreciable amount of TiC was stable till temperatures higher than 1800 K.
- Presence of Fe in the precursor powder mixture reduced the temperature range of exothermic events by about 300 ^{o}C.

- The major exothermic reactions were proven to be carbide forming reactions. The general temperature range over which reactions take place was found to be 850-1150 ^{o}C. The precise temperature range for exothermic reactions was 889-1130^{o}C with the first exothermic event occurring over a wide range of temperatures in comparison to the second event.
- The phases evolved during furnace heating of the powder mixture were TiC, M_7C_3, Fe-Cr, Fe_3C and graphite. The major phases correspond with the phases present in the spectra for laser processed plain C steel samples. Second run on the powder mixture indicated no events thus proving the thermal stability of the evolved phases.
- The laser-processed coating was found to be thermally stable till 1525 ^{o}C. The temperatures achieved due to heat build up during sliding are much lower than the temperatures 1525 ^{o}C. Hence the degradation in wear properties could be delayed due to thermal stability of the phases.
- The variation in phase evolution had strong influence on mechanical properties. The hardness and wear properties of the samples without chromium carbides were inferior to the samples with both TiC and chromium carbides.
- The formation of carbide composite surface layer provided a 5-fold improvement in the hardness (maximum hardness in coating 914 HK) of the surface (180 HK) for the as-received steel.

- The cumulative weight loss of the coating during dry sliding wear was found to be three to five times (depending on processing power) lesser than the substrate i.e. substantial improvement in the wear characteristics of the coating was observed.
- The oxidation kinetics all the carbide composite coatings followed the parabolic rate law which indicated superior oxidation resistance.

Chapter 6

6. SUGGESTIONS FOR FUTURE WORK

The present study was successful in preliminary screening of the *in-situ* carbide composite coating on AISI 1010 steel. To further investigate the coating and hence develop more fundamental and practical understanding of the system, the following can be performed.

- Transmission electron microscopy of the coating needs to be done to further investigate the presence of M_7C_3 in the coating and resolve the carbide particles. Also, mutual orientation investigations using electron microscopy with diffraction needs to be done. Since the ultra fine size of the particles made compositional analysis using SEM/EDS difficult, it is expected, with the help of TEM, it would be possible to further identify the particles in the coating.
- Preliminary investigation of the wear properties of the coating have been discussed as part of this study. Since the coating was designed for wear applications, thorough investigations using pin-on-disk wear tests needs to be done. This would also help in developing further understanding of the effect of phase variation on wear properties.
- The cohesive strength of the coating needs to be investigated to determine the fracture strength of the coating. The measurement can be performed using the four point bend test.

- Thorough investigation of oxidation behavior needs to be done by long duration exposure at elevated temperatures. This would help in observing the integrity of the coating, coating/substrate interface, phase transformations, and morphological features of the oxide scale formed on the surface.

REFERENCES

REFERENCES

[1] Sam Zhang, Deen Sun, Yongqing Fu, Hejun Du, Surface and Coatings Technology, 167, 2003, p 113.

[2] E. Pagounis, M. Talvitie and V.K. Lindroos, Metall. Trans. A, 1996, vol 27 A, pp. 4171- 4181.

[3] K.-H. Zum Gahr and G.T. Eldis: Wear, 1980, vol. 64, pp. 175-194.

[4] I. R. Sare and B. K. Arnold: Metall. Mater. Trans. A, 1995, vol 26 A, pp 357-370.

[5] Materials Science and Engineering Handbook, Edited by James F. Shackelford and William Alexander, CRC Press p.471.

[6] Materials Science and Engineering handbook, Edited by James F. Shackelford and William Alexander, CRC Press p.472.

[7] L. Bourithis, Ath. Milonas, G.D. Papadimitriou, *Surface and Coatings Technology*: 2003, vol. 165 p 286.

[8] L.E Svensson, B. Gretoft, B.Ulander and H.K.D.H. Bhadeshia, *Surface Engineering Conference*: 1985, vol 2, p 75.

[9] J.M Panchal, T.Vela, and T. Robisch: Fabrication of Particulate Reinforced Composites, ASM International, Materials Park, OH, 1990, pp 245-260.

[10] J. Kuebarsepp: Ph.D Thesis, Tallin Technical University, Tallin, 1992, pp 7-8.

[11] D.B. Miracle and H.A. Lipsitt: J.Am. Ceram. Soc., 1983, vol. 66, pp. 592-97.

[12] J.M. Panchal, T.Vela, and T. Robisch: Advances in Powder Metallurgy and Particulate Materials-1992:, Metal Powder Industries Federation and American Powder Metallurgy Institute, Princeton, NJ, 1993, vol.8, pp. 125-40.

[13] K.-W. Chae, D.-I Chun, D.-Y Kim, Y.-J. Baik, and K.-Y. Eun: J. Am. Cerac. Soc. 1990, vol 73, pp. 1979-1982.

[14] T. Z. Kattamis and T. Suganuma: Mater. Sci. Eng., 1990, vol A128, pp 241-252.

[15] B. V Chambers, T.Z. Kattamis, J.A. Cornie, and M.C. Fleming: Solidification Processing, The Institute of Metals, London, 1988, pp. 465-468.

[16] B.S.Terry, O.S. Chinyamakobvu: Mater. Sci. Technol., 1992, vol. 8, pp. 399-405.

[17] Z. Liu and H. Fredriksson: Metall. Mater. Trans. A, 1996, vol. 27A, pp 407-414.

[18] Z. Liu and H. Fredriksson: Metall. Mater. Trans. A, 1997, vol. 28A, pp 707-719.

[19] N. Frage, L. Levin, E. Manor, R. Shneck, and J. Zabicky: Scripta Mater., 1996, vol. 35, pp. 799-803.

[20] K. Murakami, A Yoshimoto, T. Okamoto, and Y. Miyamoto: Mater. Sci. and Eng., 1993, vol. A160, pp. 137-142.

[21] R. Tiwari, H.Herman, S. Sampath and B. Gudmunsson, Mater. Sci. and Eng.: A144, 1991, pp 127-131.

[22] C.C Berndt and J.H. Yi, J. Mater. Sci. For.:, 34, 1988, pp 469-473.

[23] J.T. DeMasi-Marcin and D.K. Gupta, Surf. Coat. Tech.:, Vol 68/69, 1994, p 1.

[24] V. Teixeira, M. Andritschky, W. Fisher, H.P. Buchkremer and D. Stover, Surf. Coat. Tech., 120/121, 1999, pp 103-111.

[25] G. Dearnaly and N.E.W. Hartley, Thin Film Solids, 54, 1978, p 215.

[26] J. P. Hirvonen, M. Nastasi and J.W. Mayer, Appl. Phys. Lett., 51, 1987, p 232.

[27] A. F. Baisman, S.B. Vasserman, M.G. Golkovskii, V.D. Kedo and R.A. Salimov: About Surface Hardening by Concentrated Electron beam at Atmosphere, Budker Institute of Nuclear Physics, Novosibrsk, Russia, 1988, pp 5-31.

[28] S.-H. Choo, S. Lee and S.-J Kwon: Metall. Mater. Trans.A, 1999, vol. 30 A, p 1211.

[29] M. Yan, and H. Hanqi: J. Mater. Sci., 1996, vol 31, pp. 4303-06.

[30] S. Ariely, M. Bamberger, H. Hugel, and P. Scahaaf: J Mater. Sci., 1995, vol 30, pp. 1849-1853.

[31] Annejan B. Kloosterman, Surface Modification of Titanium with Lasers. PhD thesis, Groningen University, May 1998.

[32] Frederick S. Pettit. Surface Engineering of Aluminum and Alloys, vol. 5, chapter Surface Engineering of Nonferrous Metals,. ASM International, Materials Park, Ohio, 10th edition, 1996. 2nd print, pp 784-804.

[33] M.G. Hocking, V. Vasantasree, and P.S. Sidky, Editors. Metallic and Ceramic Coatings- Production, High Temperature Properties and Applications, Longman Scientific and Technical, Harlow, Essex, England, 1st edition, 1989.

[34] Richard P. Feynman: The Feynman Lectures on Physics. Addison-Wesley Publication Company, Menlo Park, CA, 1986.

[35] Frederick Elicit Cunningham: The use of lasers for the production of surface alloys. Mechanical engineering, Massachusetts Institute of Technology, Cambridge, MA, June 1964.

[36] S Nayak, Ph.D. Dissertation University of Tennessee, Knoxville, April 2004.

[37] K. Mukherjee, Foreword: Lasers in Surface Engineering, N. B.Dahotre, editor. Surface Engineering Series, Vol. 1, ASM, Materials Park, OH, 1998.

[38]http://www.efunda.com/materials/alloys/carbon_steels/show_carbon.cfm?ID=AISI_1010&prop=all&Page_Title=AISI%201010

[39] Sidney H. Avner, in "Introduction to Physical Metallurgy" (McGraw-Hill, Singapore, 1974) 152, pp 350-356.

[40] L. Ramqvist, International J. Powder Metallurgy, 1965, 4, p 1.

[41] C. Ragunath, M.S Bhat, P.K Rohatgi, *Scripta metallurgica et Materialia*, 1995, vol 32 No.4, p. 577.

[42] J.S.Umanski and S.S. Khidekel, Zh. Fiz. Khim. SSSR, 1941, vol 15, p 983.

[43] L. Smith, J. Nutting, JISI, 1957, vol 187, pp 314-329.

[44] A.K. Seal and R. W. K Honeycombe, JISI, 1958, vol 188, pp 9-15.

[45] F.B. Pickering, 4th International Conf. On Elect. Mircos., 1958, 668, Berlin.

[46] P.H. Booker, A. O. Booker, A. O. Kunrath and M.T. Hepworth, Acta Mater., 1997 Vol. 45, No.4, pp 1625-1632.

[47] M.K. McQuillan, J. Inst. Metals, 1951, vol. 79, p 379.

[48] F. B. Cuff, N. J. Grant and C. F. Floe, Trans. AIME, 1952, vol 194, p 848.

[49] R.J Van Thyne, H.D. Kessler and M. Hansen, Trans. ASM, 1952, vol. 44, p 974.

[50] E. Rudy, D. P. Harmon and C.E. Brukl, AFML-TR-65-2, Part 1, vol. II, August 1965.

[51] A. Westgreen, G. Phragmen, and T. Negresco, JISI, 1928, vol. 117, p 386.

[52] K. Hatsuta, Kinzokyu, 1931, vol. 8, p 31.

[53] E. Friemann and F. Saurwald, Z. Anorg. Chem., 1954, vol 203, p 64.

[54] W. B.Pearson, Handbook of Lattice Spacings and Structures of Metals 2. Pergamon Press, New York, 1967.

[55] O. Rudiger, Techn. Mitt. Krupp, 1956, vol. 14, p 136.

[56] Emil N. Sobol, in "Phase Transformation and Ablation in Laser-Treated Solids", John-Wiley & Sons, NY, 1995.

[57] E. Scheil, Z. Metallkd., 1942, vol 34, p 70.

[58] M. Hillert and B. Sundman, Calphad, 1990, vol 14, pp 111-114.

[59] A.S. Khanna, Introduction to High Temperature Oxidation and Corrosion, ASM International, Materials Park, OH, 2002, pp 1-12.

[60] Seong-Hun Choo, Sunghak Lee and Soon-Ju Kwon: Metall. Trans. A, 1999, vol 30A, pp 3131-3141.

[61] Anshul Singh and Narendra B. Dahotre, Surface and interfaces in nanostructured materials, edited by S. M Mukhopadhyay, S. Seal, Narendra Dahotre, A. Agarwal, John E Smugereshy, and Neville Moody, 2004, TMS, Warrendale, PA, pp 137-141.

[62] W. Kurz and D. J Fisher, Fundamentals of Solidification (Zurich, Switzerland: TransTech Publications, Ltd., 1992)

[63] Michael E. Mullins, Erica Riley, J. Mater. Res., 4**,** No. 2, 1988, p 408.

[64] E. Pagounis, M. Talvitie and V.K. Lindroos, Metall. Trans. A, 1996, vol 27 A, pp 4183- 4191.

[65] K. Nagarathnam and K. Komvopoulos: Metall. Trans. A, 1993, vol 24A, pp 1621-1629.

[66] G.V. Samsonov and I. M Vinitskii, in "Handbook of Refractory Compounds" (IFI/Plenum Data Company, New York, 1980) pp. 140-141.

[67] B.D. Cullity, in "Elements of X-Ray Diffraction", Addison-Wesley, Philippines, 1978 p 407.

[68] Anshul Singh and N. B. Dahotre, J. Mater. Sci., in press, vol. 39, 2004, pp 1-8.

[69] S. S. Babu, R. P. Martukanitz, K. D. Parks, and S. A. David: Metall. Trans. A, 2002, vol 33A, pp 1189-1200.

[70] L.Lu, M.O. Lai, C.W Ng: Mater. Sci. and Eng.A, 1998, vol. A252, pp. 203-211.

[71] Tongxiang Fan, Z. Shi, Di Zhang, Renjie Wu: Mater. Sci. and Eng.A, 1998, vol. A257, pp. 281-286.

[72] N.B. Dahotre, M.H McCay, T. D McCay, C.R.Hubbard, W.D. Hubbard, W.D.Porter and O.B. Cavin: Scripta Met. et Mater., 1993, vol. 28, pp. 1359-1364.

[73] G. Höhne, W. Hemminger, H.-J. Flammersheim: Differential Scanning Calorimetry, Springer- Verlag Berlin Heidelberg, 1996, pp 103-105.

[74] R.D.Fraser, E.Suzuki: Analy. Chem. 1969, vol 41, pp 37-40.

VITA

Anshul Kumar Singh was born in Chandigarh, India on 20th April, 1980. He completed his B.E. (Bachelor of Engineering) in Metallurgy in June 2002 from Punjab Engineering College, Chandigarh. He worked as an intern in Hindalco Industries Ltd., Renukoot during the summer of 2000. During the summer of 2001, he carried out research on pulsed laser ablated thin films at Indian Institute of Science, Bangalore and published the results in a refereed journal. He joined the University of Tennessee, Knoxville in August 2002 as Graduate Research Assistant at the Department of Materials Science and Engineering. During his MS, he has submitted three papers each in refereed journals and conference proceedings.